# Construction of Hydrogen-Bonded Organic Ferromagnet

# (水素結合性有機強磁性体の構築)

Michio M.Matsushita

December, 1996

# Construction of Hydrogen-Bonded Organic Ferromagnet

A Thesis

Submitted to

the University of Tokyo

in Fulfillment of the Requirement

for the Degree

of

Doctor (Philosophy)

by

Michio M. Matsushita

December, 1996

# Contents

# Acknowledgment

This thesis work was carried out under the guidance of Professor Tadashi Sugawara. The author would like to thank him for his continuous interest in this work and many valuable discussion and useful advice and encouragement throughout the course of the present work.

The author wishes to thank Dr. Akira Izuoka for enlightening discussion and technical assistance.

The author would like to acknowledge Dr. Naoya Takeda and Professor Masayasu Ishikawa of Institute for Solid State Physics for the low temperature magnetic measurements.

The author gratefully acknowledges Mr. Tatsuya Kobayashi and Professor Nobuo Wada for the heat capacity measurements.

The author would like to express thanks to Professors Sadamu Takeda and Kizashi Yamaguchi of Osaka University for helpful discussion about spin distribution on HQNN molecule.

The author would like to thank Professor Norimichi Kojima for his helpful discussion especially about dimensionality of the spin system.

The author is grateful to Mr. Akira Miyazaki, Dr. Hirohiko Sato, and Professor Toshiaki Enoki of Tokyo Institute of Technology for their sincere help in SQUID measurements.

The author wishes to thank Dr. Reiji Kumai of JRCAT and Mr. Jotaro Nakazaki for their collaboration.

The author wishes to express his gratitude to all the members of this laboratory.

December, 1996

# *Chapter 1*

## Preface

Design of molecular crystals, which consist of organic molecules, is an interesting target of research from the aspect of developing novel materials carrying prominent physical properties. Whereas inorganic materials are composed of atoms which can not be modified, one can create molecular architectures by assembling various types of organic molecules by virtue of self-assembling ability, inclusion type-interaction, intercalation of guest molecules into layered-materials based on hydrogen-bond, dispersion force, charge-transfer interaction, etc. Such feasibility of constructing multi-leveled artificial structures enables us to equip organic materials with switchable multi-functionality.

Among physical properties of organic materials, conductivity and non-linear optical property have drawn much attention. Magnetism of organic materials, however, becomes a current topic.[1] This is not only because organic magnetic materials had not been existed, but also such organic magnets may be equipped with multi-functionality based on the conformational flexibility or switchablity of chemical bonds of organic

molecules, once they have been created. For instance, the origin of advanced functionalities, as spin cross-over or LIESST phenomenon, of transition metal complexes is ascribable to the structural flexibility of organic ligands towards the external field.

There are some difficulties, however, to study organic magnetic materials as described below. First, organic materials are diamagnets in general, because the electronic structure of organic molecules is of a closed-shell. In order to construct magnetic material, one has to prepare organic molecules of an open-shell structure. Although free radicals have an open-shell structure, they are unstable and exist only as reactive intermediates. The reason for the instability of organic radicals may be ascribed to the nature of the orbitals in which unpaired electrons reside. This is contrasting with transition metal ions, where unpaired electrons reside in inner-shell orbitals, such as d- or f-orbitals. Since the unpaired electron in the outer-shell is much more reactive, compared with those in the inner-shell of transition metal ions, one has to increase the kinetic stability of organic radicals through chemical modifications.

Second, it is crucial to introduce ferromagnetic intermolecular interaction. The intermolecular magnetic interaction is usually anti-ferromagnetic, because unpaired electrons in the outer-shell has a tendency to form a covalent bond, pairing unpaired electrons in an anti-ferromagnetic manner.

Therefore, in order to create organic magnetic material, one has to

prepare persistent radicals and arrange them to have ferromagnetic intermolecular interaction against the antiferromagnetic interaction which nature favors.

The study of spin alignment in organic molecules was originated by the discovery of the quintet *meta*-bisphenylmethylene.[2] The strategy of preparing high spin molecules here is to construct degenerated NBMOs based on the π-topology.[3] Along this line, tetracarbene of which spin quantum number exceeds those of transition metals has been realized.[4] Thereafter high spin polyradicals[5] and ploycarbenes[6] have been prepared. Introduction of hetero-atoms into high spin molecules have been investigated extensively in order to increase the kinetic stability of these open-shell molecules.

There is another approach to realize an organic ferromagnet by introducing ferromagnetic intermolecular interaction among organic radicals of which spin multiplicity is not necessarily large. Since antiferromagnetic interaction is favorable in radical crystals, ferromagnetic intermolecular interaction has been known only in a few cases such as galvinoxyl[7] and some of the diphenylcarbene derivatives[8] for a long time. Discovery of the first genuine organic ferromagnet, *p*-nitrophenyl nitronyl nitroxide (*p*-NPNN),[9] in 1991, stimulated the progress in this field and thereafter hundreds of ferromagnetic radical crystals have been reported.[1] Through the study of such ferromagnetic radical crystals, some organic ferromagnets, tetramethyldiazaadamantane-

dioxyl,[10] benzylideneamino-TMPO[11] were discovered successively. Over twenty organic ferromagnets have been reported at present.[9-14] In particular, the magnetic interaction in *p*-NPNN was elucidated in detail by means of magnetic susceptibility, heat capacity, μSR,[15] and neutron diffraction[16] experiments. Based on these fortuitous discoveries of organic ferromagnets, it is time to establish methodology for designing organic crystal ferromagnets.

A guiding principle concerning intermolecular magnetic interaction among organic radicals, typically for odd alternant hydrocarbons (AHC), is McConnell's theory.[17] The spin distribution of odd AHC is characterized by alternation in signs and magnitudes at each carbon atom.[18] When the spin-distributing π systems interact intermolecularly, it is an energetically favorable mode of overlap where carbon atoms having the opposite spin densities interact. Accordingly, the signs of the largest spin densities of the neighboring molecules should become the same, when the mode of overlap satisfies the topological requirement intermolecularly,[19] leading to the ferromagnetic intermolecular interaction as shown in Figure **1a**. In order to realize such a relative orientation, it is crucial to control the molecular arrangement of open-shell molecules in crystals. However, since this mechanism requests control of the molecular orientation in an angstrom scale, introduction of ferromagnetic intermolecular interaction based on this mechanism is difficult.

In this respect, the introduction of a hydrogen-bonding site into an

open-shell molecule as an orientation controlling site (Figure 1b) intrigued

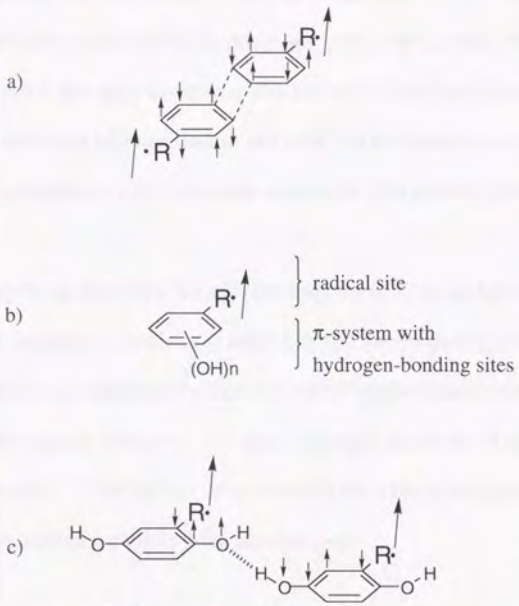


**Figure 1** a) Spin alignment of an odd alternant hydrocarbon based on McConnell's mechanism. b) Open-shell molecule with hydrogen-bonding sites. c) Ferromagnetic coupling between open-shell molecules through a hydrogen bond.

the author. Since the direction of hydrogen bond is predictable, it is often used as a method of crystal designing.[20] Hydrogen bond is supposed to be valid even in introducing the ferromagnetic interaction among organic radicals based on McConnell's mechanism. When the hydrogen bond is incorporated into the π-conjugated system, in particular, spin polarization

ought to be induced even at the hydrogen-bonding site due to the spin polarization in the π-system. As the hydrogen bond connects atoms intermolecularly at the selected positions, one can control the magnitude and the sign of the spin density at the hydrogen-bonding sites. Namely, hydrogen bond can be regarded as not only the orientation-controlling site, but also the coupler for the transmission of the spin polarization.[21]

The purpose of the thesis is to design and construction of hydrogen-bonded crystals of organic radicals and establish the methodology of controlling the intermolecular magnetic interaction based on the analysis of correlation between the crystal structure and the magnetic property of the hydrogen-bonded crystal. The author also reveals the characteristics of the spin system constructed by the crystal engineering.

This thesis is composed of the six chapters.

In chapter 2, design and preparation of free radicals having hydrogen-bonding sites (**HQNN** and **RSNN**) are described. The spin distribution on the designed radicals is discussed based on the experimental and theoretical results.

In chapter 3, the crystal structures and magnetic properties of hydrogen-bonded radical crystals, α-**HQNN**, β-**HQNN** and **RSNN** are described. The correlation between hydrogen-bonding pattern and intermolecular

interaction is discussed.

In chapter 4, the results of the magnetic measurement at lower temperatures of α-**HQNN** are described. The phase transition to the ferromagnet and the dimensionality of this spin system are documented.

In chapter 5, the isotope effect on the crystal structure and magnetic property of the hydrogen-bonded radical crystals is described by the substitution of hydrogen with deuterium. Through the changes of the crystal structure and of the magnetic property upon deuteration, the contribution of hydrogen bond to the intermolecular interaction is revealed.

In chapter 6, the future scope of hydrogen-bonded type organic magnets is discussed.

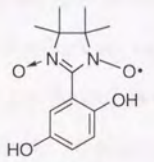


**HQNN**

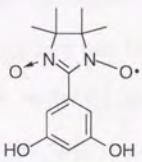


**RSNN**

# *Chapter 2*

Design and Preparation of Stable Free Radicals Bearing Hydrogen-Bonding Sites

---

## 2.1. Design of stable radicals bearing hydrogen-bonding sites

Phenyl nitronyl nitroxide (**PhNN**)[22] is a famous stable free radical and the spin distribution of it has been investigated in detail by ESR,[23] NMR,[24] neutron diffraction experiment,[25] and theoretical calculation.[26] The characteristics of the spin distribution are as follows (Figure 2-1a): First, most of the spin densities are equally shared by two NO groups. Second, a large negative spin density is observed on the C1 atom between the two NO groups. Third, an alternation in the spin densities on the carbon atoms of the phenyl ring is noted. Fourth, the methyl protons of the NN groups have significant negative spin densities, derived from the positively polarized methyl carbons (Figure 2-1b).

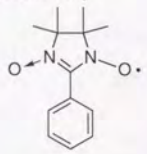

**PhNN**

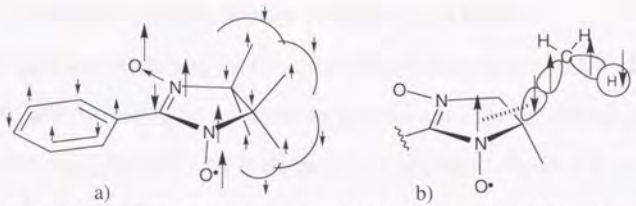


**Figure 2-1.** a) Spin distribution on the phenyl nitronyl nitroxide. b) Spin polarization at the methyl hydrogen of nitronyl nitroxide derived from a hyper-conjugation between the $\pi$ radical and the C-C bond.

To form hydrogen-bonded crystals, hydroxy groups are introduced as the hydrogen-bonding site to the PhNN at the benzene ring. Since the designed **PhNN** derivatives have a hydroquinone (**HQ**) or a resorcinol (**RS**) moiety, these radicals are named **HQNN**[12] and **RSNN**,[13,27] respectively. In **HQNN**, two hydroxy groups are introduced at 2'- and 5'-positions carrying negative and positive spin densities, respectively.[28] If the intermolecular hydrogen bond is formed between these two sites, the spin polarization may be transmitted along the hydrogen bond, leading to the ferromagnetic intermolecular interaction. On the other hand, the magnetic interaction in **RSNN** may be opposite to the previous case, because the hydroxy groups are introduced at 3'- and 5'-carbons which carry positive spin densities.

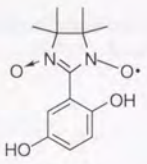

**HQNN**

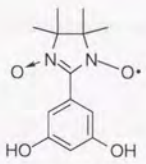

**RSNN**

## 2.2. Calculated spin distribution of HQNN and RSNN

The spin distribution on the dihydroxyphenyl nitronyl nitroxides (**HQNN**, **RSNN**) was estimated by the semi-empirical molecular orbital calculation (MOPAC MNDO-PM3 / UHF method)[29] as shown in Figure 2-2. In both HQNN and RSNN, oxygens and nitrogens of the NN group have large positive spin densities suggesting that the unpaired electron is mostly localized at these sites. The α carbon of NN group has the negative spin density. While the positive and negative spin densities distribute alternatively over the benzene ring. These features are similar to the spin distribution of PhNN determined by the neutron diffraction experiment.

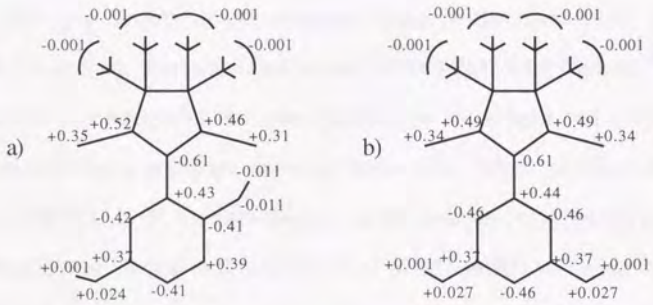


**Figure 2-2.** Spin distribution on the nitronyl nitroxide derivatives calculated by PM3/UHF method. a) HQNN b) RSNN

The hydroxy groups of HQNN are spin-polarized in the same sign as those of the ipso carbon atoms of the benzene ring. Namely, the hydroxy group at 2'- position of HQNN is spin-polarized negatively, while that of 5'-position is polarized positively[28] as shown in Figure 2-3. On the other hand, both hydroxy groups at 3'- and 5'-positions of RSNN are spin-polarized positively.

a) 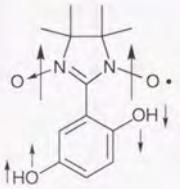


b) 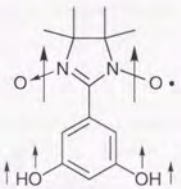


**Figure 2-3.** a) Signs of spin densities on the hydroxy groups of HQNN. b) Signs of spin densities on the hydroxy groups of RSNN.

The spin density on the hydroxy group in the model spin system, $CH_2OH$ radical, was calculated by the MNDO-PM3/UHFmethod.[29] The angular dependence of the spin densities on an oxygen and a hydrogen atom of hydroxy group are shown in Figure 2-4. When the dihedral angel, $\theta = \angle HCOH$, is 0°, the spin density on the hydrogen atom of the hydroxy group is nearly equal to 0, and increased to 0.08 at 90° following the $\sin^2\theta$ relation. On the contrary, the spin density on the oxygen atom is 0.10 at 0°, and it decreases following the $\cos^2\theta$ relation. It falls to -0.04 at 90° crossing zero at around 60°. According to this result, both the hydrogen and the oxygen atoms of the hydroxy group have the same sign of spin densities as the *ipso* carbon atom in the dihedral angle range of 0°-60°.

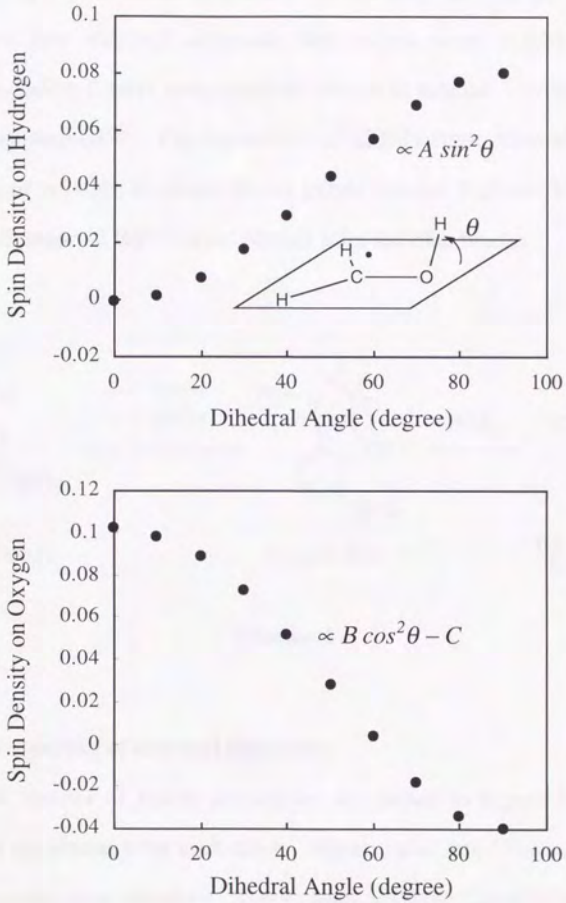


**Figure 2-4.** Angular dependence of the spin densities on a hydrogen atom and an oxygen atom of the hydroxy group of $CH_2OH$ radical.

## 2.3. Preparation of nitronyl nitroxides having hydroxy groups

Two new nitronyl nitroxide derivatives were synthesized from corresponding formyl compounds as shown in scheme 1 according to the ordinary method.[22] Crystallization of HQNN from ether afforded two phases of crystals; α-phase: bluish purple blocks, β-phase: blue needles. Crystallization of RSNN from ethanol afforded blue blocks.

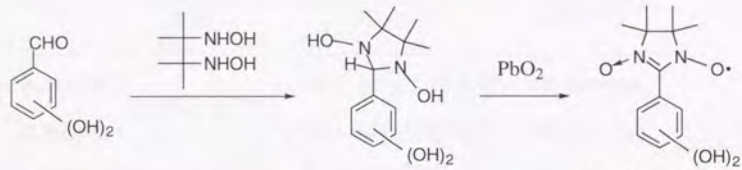


**2(a 2,5 b 3,5)** **3(a 2,5 b 3,5)** **1(a 2,5 = HQNN b 3,5 = RSNN)**

**Scheme 1**

## 2.4. Properties of nitronyl nitroxides

ESR spectra of PhNN derivatives are shown in Figure 2-5. These spectra are almost same each other. Signals splits into 5 lines according to the two equivalent nitrogens. The g values and hyperfine coupling constants of HQNN and RSNN in benzene are listed in table 2-I, together with OH stretching frequencies in IR spectra and melting points. The OH stretching bands are observed in two regions. One is at around 3300 $cm^{-1}$, and the

other is between 3200 and 2500 $cm^{-1}$. The tendency suggests the presence of two types of hydrogen bonds. The former may be assigned to the intermolecular hydrogen bond, and the latter is to the intramolecular one. While two absorption bands of RSNN are in the region of the intermolecular hydrogen bond.

**Table 2-I.** ESR g-factor, hyperfine coupling constant, OH stretching frequency, and melting point of α-HQNN, β-HQNN and RSNN.

| | ESR[a] | | IR ($cm^{-1}$)[b] | m.p. (°C) |
|---|---|---|---|---|
| | g | $a_N$ (mT) | | |
| **α-HQNN** | 2.0061 | 0.756 | 3264, 3200-2500 (O-H) | 109 (decomp) |
| **β-HQNN** | | | 3324, 3200-2500 (O-H) | 108 (decomp) |
| **RSNN** | 2.0063 | 0.748 | 3312, 3208 (O-H) | 75 |

a) In benzene solution. b) KBr pellet

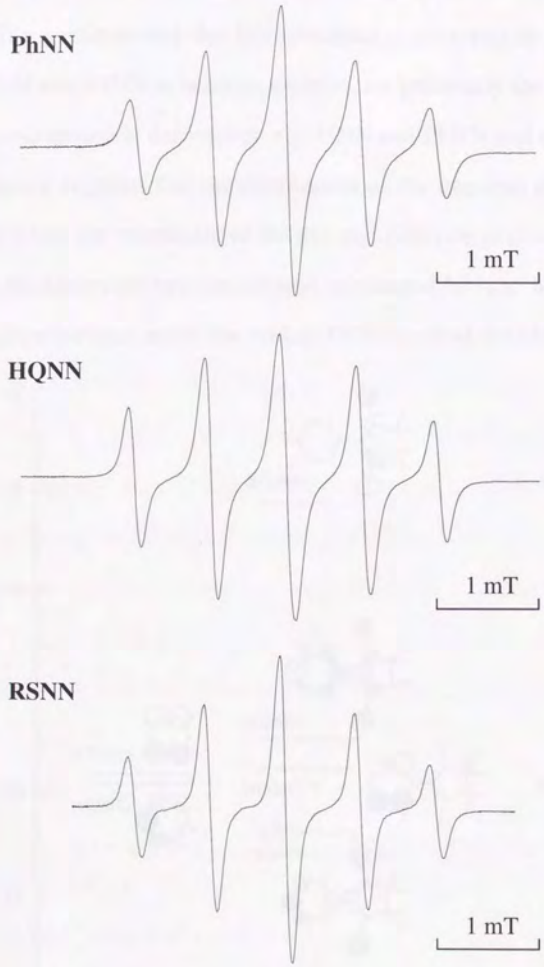


**Figure 2-5.** ESR spectra of **PhNN**, **HQNN**, and **RSNN** in Benzene.

## 2.5. Spin distribution of nitronyl nitroxides

The g-values and the hfs parameters, observed in ESR spectra of HQNN and RSNN in benzene solution, are practically the same as those of nitronyl nitroxide derivatives, *e.g.* HNN and PhNN and others.[22,23] The tendency suggests that the distribution of the unpaired electron does not alter when the substituent of the nitronyl nitroxide is changed. Provided that the electronic structure of aryl-substituted NN can be represented by the perturbational molecular orbital (PMO) method, the above tendency

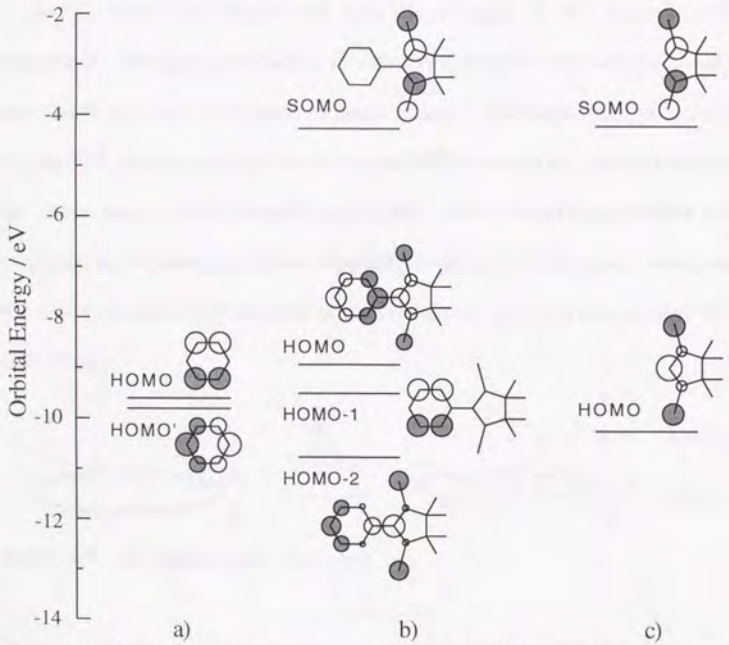


**Figure 2-6.** Molecular orbital diagram: a) Benzene b) PhNN c) HNN.

may be rationalized as follows. The *somo* of the NN group has $a_2$ local symmetry due to the presence of the $C_2$ symmetry axis, whereas the symmetry of the partial molecular orbital of the substituent is not necessarily $a_2$. Thus *somo* of the NN group becomes *somo* of the entire molecule without being perturbed. Even when the symmetry of two units, the NN group and the substituent, coincides, the perturbation between two units should be subtle, because the coefficient at C1 of the NN group of *somo* is negligibly small.

Nevertheless the significant spin distribution on the phenyl ring is observed. The spin distribution in nitronyl nitroxide derivatives should be derived from "spin polarization" mechanism. Although *somo* is localized on the NN group, most of the occupied MOs, which are located between the *somo*, spread over the entire molecule. Since the occupied MOs share coefficients of atomic orbitals which belong to the NN group with *somo*, the spin polarization is induced at the NN group, and it is transmitted to the phenyl ring.

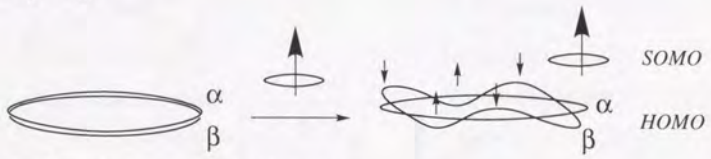


**Figure 2-7.** An image of spin polarization.

The spin polarization in PhNN derivatives is smaller compared with that of odd alternant hydrocarbons in which an unpaired electron is delocalized over the entire molecule, significant spin polarization in the phenyl group is estimated by the semi-empirical MO calculation. The values, however, are much larger than those determined by the neutron diffraction experiment. The calculated spin polarization is considered to be overestimated, although the sign of spin densities is in accord with the experimental result. In order to estimate the accurate spin polarization, more sophisticated MO calculation should be required.

The spin polarization of the hydroxy groups in HQNN or RSNN is found to be always the same as that of *ipso*-carbons of the phenyl ring. This result should be derived from the contribution of the hyper-conjugation between the π-spin on the *ipso* carbon atom and the lone pairs of electrons of the oxygen atom or the OH bond (**Figure 2-8**).

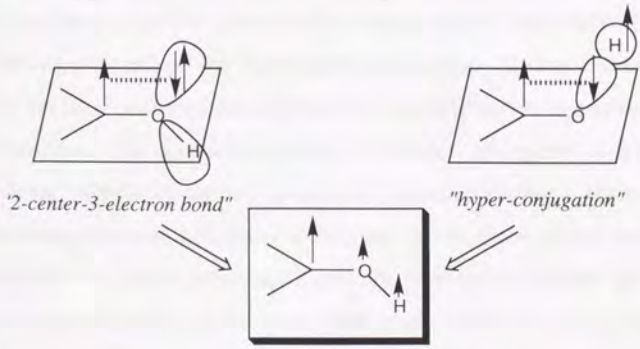


**Figure 2-8.** Spin-induction mechanism at an oxygen atom and a hydrogen atom of the hydroxy group.

## 2.6. Experimental

**Materials.**

**HQNN(2-(2',5'-dihydroxyphenyl)-4,4,5,5-tetramethyl-4,5-dihydro-1*H*-imidazolyl-1-oxyl-3-oxide) (1a).** In a 100 ml round-bottom flask was placed 1.94 g of 2,5-dihydroxybenzaldehyde (**2a**) (14 mmol), 1.80 g of 2,3-dimethyl-2,3-dihydroxyl-aminobutane[30] (12 mmol), 0.07 g of 2,3-dimethyl-2,3-dihydroxylaminiumbutane sulfonate (catalyst), and 4 g of crushed 3 A molecular sieves under a nitrogen atmosphere. To this mixture was added 50ml of benzene containing 5% of methanol. After stirring 4 days, the solvent was removed by evaporation and then added 50ml of $CHCl_3$ and filtered. The residue was washed with $CHCl_3$ twice over a filter, and the condensation product was extracted with THF. After evaporation, the cyclic bishydroxylamine (**3a**) was obtained as white powder.; 2.86 g (88%). NMR (270 MHz, Acetone-$d_6$), $\delta$ = 7.42 ( 1H, br.s, -OH); 6.71 ( 1H, d, J=2.93Hz, Ar-H); 6.61 ( 1H, dd, J=2.93, 8.79, Ar-H); 6.50 (1H, d, J=8.42, Ar-H); 4.68 ( 1H, s, methine-H); 1.20 ( 6H, s, methyl-H); 1.14ppm ( 6H, s, methyl-H). Under a nitrogen atmosphere, 208 mg of **3a** (cyclic bishydroxylamine) (7.8mmol) was placed in a 50 ml round bottomed flask. Dried THF of 10 ml was added, and the mixture was stirred at room temperature. A mixture of 1.0 g of $PbO_2$ and 200 mg of crushed molecular sieves(3A) was added into the solution and stirred for 10 minutes. The solution was filtered off through a celite-pad to yield a dark blue solution. After condensation, the oxidized product was purified by silica-gel column chromatography with diethylether as an eluant. Fractions colored blue were collected and dried over sodium sulfate and filtered off. A purple oil (**HQNN**, **1a**) of 170 mg was obtained by removing the solvent; 88% yield. ESR (Benzene): g = 2.0061, $a_N$ = 0.756 mT(2N). Mass. (FAB): Obs. $M+1^+$ = 266 (Cal. $C_{13}H_{17}N_2O_4$ = 265). UV (THF): $\lambda$max = 347( $\varepsilon$ > 7000 ); 580( $\varepsilon$ = 410 ); 630 nm( $\varepsilon$= 270 ). **Crystallization of**

**HQNN.** Purple oil of HQNN was mixed with 30 ml of diethylether. Then the dark blue solution was stored in a refrigerator (≈ 4°C) under a nitrogen atmosphere. After four hours, block shaped blue-purple crystals (α-phase), ca. 0.2 × 0.4 × 0.2mm in sizes, were obtained. When the solution was stored in a freezer (≈ −10°C), needle shaped crystals (β-phase) were obtained. Both phases can be obtained selectively by using a seed crystal at room temperature. **α-phase crystal.** IR(KBr): 3270(OH); 1480, 1332 $cm^{-1}$(nitronyl nitroxide); E.A. Calcd. for $C_{13}H_{17}N_2O_4$: C 58.85; H 6.46; N 10.56 (%). Found: C 58.89; H 6.47; N 10.54 (%); m.p.: 109 °C (decomp). **β-phase crystal.** IR(KBr): 3320(OH); 1489, 1456, 1426, 1326 $cm^{-1}$ (nitronyl nitroxide); E.A. Calcd. for $C_{13}H_{17}N_2O_4$: C 58.85; H 6.46; N 10.56 (%). Found: C 58.78; H 6.46; N 10.53 (%); m.p.: 108 °C(decomp).

**RSNN (2-(3',5'-dihydroxyphenyl)-4,4,5,5-tetramethyl-4,5-dihydro-1*H*-imidazolyl-1-oxyl-3-oxide) (1b).** In a 30 ml round bottom flask was placed 0.244 g of 3,5-dihydroxybenzaldehyde (**2b**) (1.8mmol), 0.243 g of 2,3-dimethyl-2,3-dihydroxyl–aminobutane (1.7mmol), 66 mg of 2,3-dimethyl-2,3-dihydroxylaminiumbutane sulfonate, and 1 g of crushed molecular sieves (3A), under a nitrogen atmosphere. To this mixture was added 20 ml of benzene containing 5 % of methanol. After stirring 3 days, the solvent was removed by evaporation. The residue was washed with $CHCl_3$ twice over a filter, and the crude condensation product was extracted with THF. After evaporation, the cyclic bishydroxylamine (**3b**) was obtained as white powder.; 0.371 g (83%). NMR (270MHz,DMSO-$d_6$), δ = 8.96 ( 2H, d, J = 3.3 Hz, -OH); 7.66 ( 2H, d, J = 3.48 Hz, N-OH); 6.37 ( 2H, d, J = 2.38 Hz, Ar-H); 6.07 (1H, s, Ar-H); 4.27 ( 1H, d, methine-H); 1.02 ( 12H, t, methyl-H). Under a nitrogen atmosphere, 0.371 g of the cyclic bishydroxylamine (1.38 mmol) was placed in a 100 ml round bottomed flask. Dried THF of 60 ml was added into the flask and stirred. A mixture of 2.5 g of $PbO_2$ and 1 g of crushed molecular sieves (3A) was added into the solution and stirred for 4

hours. The solution was filtered off through celite-pad to yield a dark blue solution. After condensation, the oxidized product was purified by silica-gel column chromatography with ethylacetate as an eluant. A blue fraction was collected and dried over sodium sulfate and filtered off. The obtained crude crystals were dissolved in ethyl acetate and stored in refrigerator (≈ 4°C) under a nitrogen atmosphere. Blue plates were obtained; 170 mg (46 %). IR(KBr): 3311, 3207(OH); 1372, 1343 $cm^{-1}$(nitronylnitroxide); E.A. Calcd. for $C_{13}H_{17}N_2O_4$: C 58.85; H 6.46; N 10.56 (%). Found: C 58.63; H 6.42; N 10.30 (%); m.p.: 75°C. ESR (benzene): g = 2.0063, $a_N$ = 0.748 mT(2N).

**Instrumentation.** $^1$H NMR spectra were measured by JEOL GSH-270 (270MHz) spectrometer, on which chemical shifts in deuterated solutions were reported in δ relative to $Me_4Si$ as an internal standard. Infra-Red spectra were recorded by Perkin-Elmer 1640 FTIR spectrometer using a KBr pellet. UV-Vis absorption spectra were obtained on Shimazu UV-3100PC spectrometer. ESR measurement were carried out with an X-band ( 9.4 GHz ) ESR spectrometer (JEOL JES-RE2X), with a modulation of 100 kHz. Resonance fields were measured by an NMR field meter (JEOL ES-FC5). Frequency of microwave was recorded by an ADVANTEST TR5212 frequency counter.

# *Chapter 3*

## Crystal Structures and Magnetic Properties of the Crystals of Nitronyl Nitroxides Having Hydroxy Groups

### 3.1. Introduction

Phenyl nitronyl nitroxide derivatives substituted with hydroxy groups (**HQNN**[12] and **RSNN**[13,27]) were designed and prepared to form hydrogen-bonded crystals. In HQNN, two hydroxy groups are introduced at 2'- and 5'-positions carrying negative and positive spin densities, respectively. If the intermolecular hydrogen bond is formed between these two sites, the spin polarization may be transmitted along the hydrogen bond, leading to the ferromagnetic intermolecular interaction. On the other hand, the magnetic interaction in RSNN may be opposite to the previous case, because the hydroxy groups are introduced at 3'- and 5'-carbons which carry positive spin densities. In this respect, the crystal structure determination and magnetic measurement of these nitronyl nitroxide derivatives were carried out .

### 3.2. Crystal Structures

The crystal structures of α-HQNN, β-HQNN and RSNN were revealed by X-ray crystallography. The crystallographic parameters are listed in Table 3-I. Molecular structures and selected bond lengths and angles are given in Figure 3-1 and Table 3-V, respectively. Crystal packing of α-HQNN, β-HQNN and RSNN are shown in Figures 3-2/3, 3-4, and 3-5, respectively. Geometries of the hydrogen bonds with selected intermolecular contacts of α-HQNN, β-HQNN and RSNN are summarized in Tables 3-VI, 3-VII, and 3-VIII, respectively.

**Table 3-I.** Crystallographic parameters of α-HQNN, β-HQNN and RSNN.

| crystal | **α–HQNN** | **β–HQNN** | **RSNN** |
|---|---|---|---|
| molecular weight | 265.29 | 265.29 | 265.29 |
| space group | $P2_1/n$ | $P2_1/a$ | $P2_1/n$ |
| $a$, Å | 15.142(3) | 10.586(3) | 9.817(2) |
| $b$, Å | 12.320(1) | 14.072(2) | 19.817(4) |
| $c$, Å | 7.196(1) | 9.744(2) | 6.993(1) |
| $\beta$, deg | 99.18(2) | 113.89(1) | 108.07(1) |
| $V$, Å$^3$ | 1325.3(4) | 1327.3(5) | 1293.4(4) |
| $Z$ | 4 | 4 | 4 |
| $T$, °C | 25 | 25 | 25 |
| $\rho$, g cm$^{-1}$ | 1.331 | 1.333 | 1.366 |
| Reflections | 2204 | 1596 | 2220 |
| Parameters | 240 | 240 | 240 |
| $R$ | 0.051 | 0.049 | 0.047 |
| $R_W$ | 0.047[a] | 0.048[b] | 0.047[c] |

a) $W = 1.0$ ($|F_o|<20$), $0.7$ ($20 \le |F_o| < 60$), $200/|Fo|^2$ ($60 \le |F_o|$)
b) $W = 1.0$ ($|F_o|<50$), $200/|Fo|^2$ ($50 \le |F_o|$)
c) $W = 1.0$ ($|F_o|<30$), $500/|Fo|^2$ ($30 \le |F_o|$)

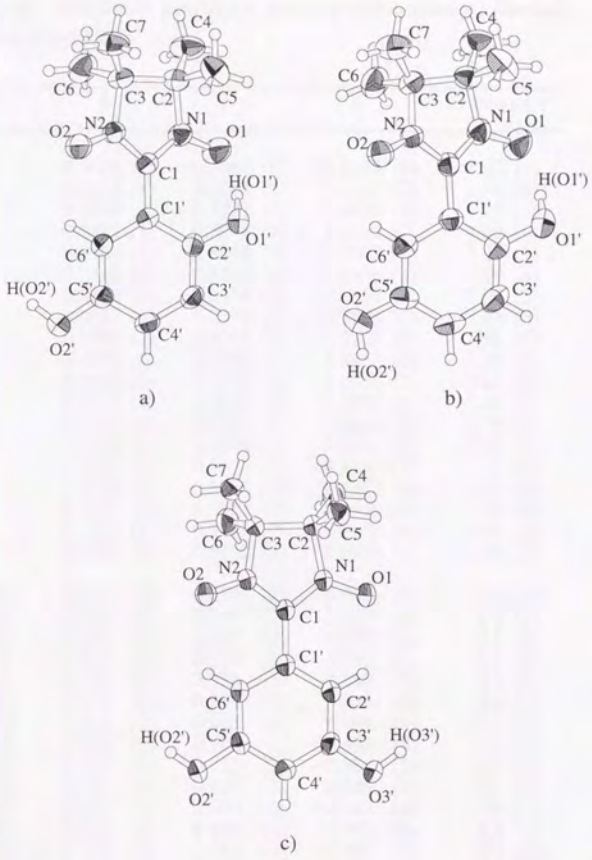


**Figure 3-1.** ORTEP drawing (50% probability) of molecular structures with atomic numbering scheme: a) α-HQNN b) β-HQNN c) RSNN

**Table 3-II.** Positional parameters and equivalent isotropic thermal parameters of α-HQNN.

| atom | *x* | *y* | *z* | *B*eq (Å$^2$) |
|---|---|---|---|---|
| O1' | 0.0628 (1) | 0.3342 (1) | 0.5619 (2) | 3.62 (4) |
| O2' | -0.0281 (1) | 0.2284 (1) | 1.2525 (2) | 4.48 (4) |
| O1 | 0.0958 (1) | 0.5327 (1) | 0.6058 (2) | 4.71 (4) |
| O2 | 0.2532 (1) | 0.3974 (1) | 1.1617 (2) | 4.47 (4) |
| N1 | 0.1581 (1) | 0.5163 (1) | 0.7503 (2) | 3.27 (4) |
| N2 | 0.2310 (1) | 0.4555 (1) | 1.0156 (2) | 3.09 (4) |
| C2' | 0.0396 (1) | 0.3154 (2) | 0.7350 (3) | 2.94 (5) |
| C3' | -0.0255 (1) | 0.2379 (2) | 0.7496 (3) | 3.44 (5) |
| C4' | -0.0460 (1) | 0.2091 (2) | 0.9229 (3) | 3.49 (5) |
| C5' | -0.0034 (1) | 0.2599 (2) | 1.0857 (3) | 3.25 (5) |
| C6' | 0.0605 (1) | 0.3383 (2) | 1.0736 (3) | 3.14 (5) |
| C1' | 0.0831 (1) | 0.3666 (2) | 0.8979 (3) | 2.80 (4) |
| C1 | 0.1544 (1) | 0.4448 (1) | 0.8876 (2) | 2.79 (4) |
| C2 | 0.2480 (1) | 0.5684 (2) | 0.7611 (3) | 3.39 (5) |
| C3 | 0.2843 (1) | 0.5532 (2) | 0.9737 (3) | 3.29 (5) |
| C4 | 0.2982 (2) | 0.5023 (2) | 0.6313 (4) | 5.27 (8) |
| C5 | 0.2367 (2) | 0.6851 (2) | 0.6939 (4) | 5.10 (7) |
| C6 | 0.3837 (1) | 0.5273 (2) | 1.0177 (4) | 5.03 (7) |
| C7 | 0.2603 (2) | 0.6450 (2) | 1.0976 (4) | 5.24 (7) |
| H(O1') | 0.070 (2) | 0.410 (2) | 0.553 (4) | 7.4 (7) |
| H(O2') | -0.000 (2) | 0.270 (2) | 1.344 (4) | 8.2 (7) |
| H(C3') | -0.056 (1) | 0.201 (2) | 0.638 (2) | 4.1 (5) |
| H(C4') | -0.090 (1) | 0.153 (2) | 0.931 (3) | 4.1 (5) |
| H(C6') | 0.091 (1) | 0.376 (2) | 1.187 (3) | 4.3 (5) |
| H(C4)1 | 0.357 (2) | 0.537 (2) | 0.628 (4) | 6.8 (7) |
| H(C4)2 | 0.313 (2) | 0.425 (2) | 0.685 (4) | 7.0 (7) |
| H(C4)3 | 0.262 (2) | 0.500 (2) | 0.509 (4) | 6.8 (7) |
| H(C5)1 | 0.197 (2) | 0.726 (2) | 0.767 (3) | 6.4 (6) |
| H(C5)2 | 0.289 (2) | 0.722 (2) | 0.722 (4) | 6.4 (6) |
| H(C5)3 | 0.213 (2) | 0.690 (2) | 0.563 (4) | 7.5 (7) |
| H(C6)1 | 0.399 (2) | 0.460 (2) | 0.947 (4) | 6.5 (7) |
| H(C6)2 | 0.415 (2) | 0.587 (2) | 0.981 (4) | 6.7 (7) |
| H(C6)3 | 0.398 (2) | 0.519 (2) | 1.151 (4) | 6.6 (7) |
| H(C7)1 | 0.198 (2) | 0.658 (2) | 1.079 (3) | 5.8 (6) |
| H(C7)2 | 0.293 (2) | 0.714 (2) | 1.069 (4) | 7.2 (7) |
| H(C7)3 | 0.282 (2) | 0.627 (2) | 1.229 (4) | 7.1 (7) |

**Table 3-III.** Positional parameters and equivalent isotropic thermal parameters of β-HQNN.

| atom | *x* | *y* | *z* | *B*eq (Å$^2$) |
|---|---|---|---|---|
| O1' | 0.2092 (2) | 0.9402 (2) | 0.6301 (3) | 6.0 (1) |
| O2' | 0.3797 (3) | 1.3142 (2) | 0.7394 (3) | 6.0 (1) |
| O1 | 0.4200 (2) | 0.8593 (2) | 0.8438 (3) | 6.0 (1) |
| O2 | 0.6468 (2) | 1.0723 (2) | 0.6630 (3) | 4.9 (1) |
| N1 | 0.5131 (3) | 0.8987 (2) | 0.8081 (3) | 4.0 (1) |
| N2 | 0.6247 (2) | 1.0021 (2) | 0.7336 (3) | 3.4 (1) |
| C2' | 0.2554 (3) | 1.0314 (2) | 0.6617 (4) | 3.9 (1) |
| C3' | 0.1573 (3) | 1.1030 (3) | 0.6296 (4) | 4.5 (1) |
| C4' | 0.1967 (3) | 1.1969 (3) | 0.6514 (4) | 4.2 (1) |
| C5' | 0.3345 (3) | 1.2218 (2) | 0.7094 (4) | 4.1 (1) |
| C6' | 0.4323 (3) | 1.1520 (2) | 0.7444 (4) | 3.8 (1) |
| C1' | 0.3944 (3) | 1.0560 (2) | 0.7191 (4) | 3.3 (1) |
| C1 | 0.5047 (3) | 0.9869 (2) | 0.7507 (3) | 3.2 (1) |
| C2 | 0.6364 (3) | 0.8449 (2) | 0.8101 (4) | 3.7 (1) |
| C3 | 0.7313 (3) | 0.9288 (2) | 0.8140 (4) | 3.5 (1) |
| C4 | 0.6911 (4) | 0.7790 (3) | 0.9442 (5) | 5.6 (1) |
| C5 | 0.5861 (5) | 0.7895 (3) | 0.6642 (4) | 5.9 (2) |
| C6 | 0.8267 (4) | 0.9123 (3) | 0.7358 (5) | 5.6 (2) |
| C7 | 0.8113 (4) | 0.9687 (3) | 0.9711 (4) | 5.4 (1) |
| H(O1') | 0.064 (3) | 1.085 (2) | 0.589 (4) | 6.3 (9) |
| H(O2') | 0.126 (3) | 1.242 (2) | 0.625 (3) | 5.3 (8) |
| H(C3') | 0.526 (3) | 1.166 (2) | 0.783 (3) | 4.4 (7) |
| H(C4') | 0.773 (4) | 0.754 (3) | 0.949 (4) | 8.2 (11) |
| H(C6') | 0.627 (4) | 0.727 (3) | 0.936 (4) | 7.9 (10) |
| H(C4)1 | 0.710 (4) | 0.814 (3) | 1.038 (4) | 8.7 (12) |
| H(C4)2 | 0.556 (3) | 0.833 (2) | 0.572 (4) | 5.8 (8) |
| H(C4)3 | 0.666 (4) | 0.755 (3) | 0.653 (4) | 7.7 (10) |
| H(C5)1 | 0.519 (4) | 0.746 (3) | 0.666 (4) | 7.9 (10) |
| H(C5)2 | 0.773 (4) | 0.898 (3) | 0.629 (4) | 7.1 (10) |
| H(C5)3 | 0.870 (4) | 0.966 (3) | 0.736 (4) | 7.6 (10) |
| H(C6)1 | 0.885 (3) | 0.857 (2) | 0.780 (4) | 5.6 (8) |
| H(C6)2 | 0.754 (4) | 0.976 (2) | 1.027 (4) | 7.0 (9) |
| H(C6)3 | 0.848 (3) | 1.031 (2) | 0.967 (4) | 6.2 (9) |
| H(C7)1 | 0.880 (4) | 0.921 (3) | 1.030 (4) | 7.6 (10) |
| H(C7)2 | 0.272 (4) | 0.904 (3) | 0.703 (4) | 8.7 (11) |
| H(C7)3 | 0.307 (5) | 1.352 (4) | 0.709 (6) | 13.2 (16) |

**Table 3-IV.** Positional parameters and equivalent isotropic thermal parameters of RSNN.

| atom | *x* | *y* | *z* | *B*eq (Å$^2$) |
|---|---|---|---|---|
| O1 | 0.8878 (2) | 0.4142 (1) | 0.0317 (2) | 4.0 (1) |
| O2 | 0.4911 (2) | 0.4440 (1) | 0.2457 (3) | 4.2 (1) |
| O3' | 1.0542 (2) | 0.6302 (1) | 0.3063 (3) | 4.3 (1) |
| O2' | 0.7660 (2) | 0.6061 (1) | 0.7236 (2) | 4.3 (1) |
| N1 | 0.7673 (2) | 0.4052 (1) | 0.0629 (2) | 2.7 (1) |
| N2 | 0.5828 (2) | 0.4174 (1) | 0.1708 (2) | 2.8 (1) |
| C1' | 0.7771 (2) | 0.5046 (1) | 0.2897 (3) | 2.7 (1) |
| C2' | 0.8836 (2) | 0.5392 (1) | 0.2355 (3) | 2.9 (1) |
| C3' | 0.9487 (2) | 0.5942 (1) | 0.3490 (3) | 2.9 (1) |
| C4' | 0.9096 (2) | 0.6154 (1) | 0.5135 (3) | 3.0 (1) |
| C5' | 0.8021 (2) | 0.5815 (1) | 0.5636 (3) | 2.9 (1) |
| C6' | 0.7354 (2) | 0.5261 (1) | 0.4543 (3) | 2.8 (1) |
| C1 | 0.7106 (2) | 0.4446 (1) | 0.1767 (3) | 2.6 (1) |
| C2 | 0.6661 (2) | 0.3511 (1) | -0.0462 (3) | 2.7 (1) |
| C3 | 0.5642 (2) | 0.3472 (1) | 0.0850 (3) | 2.8 (1) |
| C4 | 0.5942 (2) | 0.3790 (1) | -0.2568 (3) | 3.9 (1) |
| C5 | 0.7477 (3) | 0.2869 (1) | -0.0551 (4) | 4.1 (1) |
| C6 | 0.6168 (3) | 0.2995 (1) | 0.2650 (4) | 4.2 (1) |
| C7 | 0.4088 (2) | 0.3334 (1) | -0.0314 (4) | 4.1 (1) |
| H(C2') | 0.912 (2) | 0.525 (1) | 0.121 (3) | 3.7 (5) |
| H(C4') | 0.954 (2) | 0.652 (1) | 0.593 (3) | 2.8 (4) |
| H(C6') | 0.662 (2) | 0.504 (1) | 0.492 (3) | 3.5 (5) |
| H(C4)1 | 0.525 (3) | 0.347 (1) | -0.333 (4) | 5.3 (6) |
| H(C4)2 | 0.670 (3) | 0.386 (1) | -0.322 (4) | 5.4 (6) |
| H(C4)3 | 0.534 (3) | 0.423 (1) | -0.255 (4) | 5.2 (6) |
| H(C5)1 | 0.811 (3) | 0.295 (1) | -0.137 (4) | 5.8 (7) |
| H(C5)2 | 0.683 (3) | 0.251 (1) | -0.104 (4) | 5.9 (6) |
| H(C5)3 | 0.812 (3) | 0.271 (1) | 0.090 (5) | 6.7 (7) |
| H(C6)1 | 0.615 (3) | 0.251 (1) | 0.226 (4) | 4.8 (6) |
| H(C6)2 | 0.719 (3) | 0.306 (1) | 0.347 (4) | 5.4 (6) |
| H(C6)3 | 0.553 (3) | 0.303 (1) | 0.346 (4) | 4.7 (6) |
| H(C7)1 | 0.404 (3) | 0.293 (1) | -0.104 (4) | 5.7 (6) |
| H(C7)2 | 0.358 (3) | 0.329 (1) | 0.066 (4) | 5.4 (6) |
| H(C7)3 | 0.365 (3) | 0.371 (1) | -0.133 (4) | 5.8 (6) |
| H(O1') | 1.067 (3) | 0.615 (2) | 0.191 (5) | 7.2 (8) |
| H(O2') | 0.684 (3) | 0.588 (1) | 0.729 (4) | 6.6 (7) |

**Table 3-V.** Selected bond lengths (Å) and angles (deg) of α-HQNN, β-HQNN, and RSNN.

| Bonds or Angles | **α-HQNN** | **β-HQNN** | **RSNN** |
|---|---|---|---|
| O1-N1 | 1.303(2) | 1.296(4) | 1.280(2) |
| O2-N2 | 1.272(2) | 1.279(4) | 1.287(3) |
| C1-N1 | 1.332(2) | 1.350(5) | 1.353(3) |
| C1-N2 | 1.367(2) | 1.364(5) | 1.355(3) |
| C1-C1' | 1.457(3) | 1.454(5) | 1.464(3) |
| O1'-C2' | 1.367(2) | 1.364(5) | 1.365(3) |
| O3'-C3' | ——— | ——— | 1.364(3) |
| O2'-C5' | 1.370(3) | 1.376(5) | ——— |
| O1'-H(O1') | 0.95(3) | 0.91(4) | 0.84(3) |
| O2'-H(O2') | 0.89(3) | 0.88(6) | ——— |
| O3'-H(O3') | ——— | ——— | 0.89(3) |
| N1-C1-N2 | 107.7(2) | 106.7(3) | 107.4(2) |
| C1-N1-O1 | 125.7(2) | 125.1(3) | 126.2(2) |
| C1-N2-O2 | 125.9(2) | 124.7(3) | 125.6(2) |
| C1-N1-C2 | 113.0(2) | 112.3(3) | 112.6(2) |
| C1-N2-C3 | 111.5(2) | 111.8(3) | 112.2(2) |
| Arom ring-O1'-H(O1') | 43(2) | 36(3) | 5(2) |
| Arom ring-O2'-H(O2') | 4(2) | 3(4) | ——— |
| Arom ring-O3'-H(O3') | ——— | ——— | 13(2) |
| Arom ring-NN plane | 37.2(1) | 37.2(1) | 23.3(1) |

In α-HQNN, an asymmetric unit comprises one molecule and the unit cell contains four molecules with a space group of $P2_1/n$. The phenolic hydroxy group H(O1') forms a strong intramolecular hydrogen bond (O1'•••O1 2.507 (2) Å) with the NN group (N1-O1) (Table 3-VI). This hydrogen bond causes a bond alternation of the NN group: the O1-N1 and C1-N1 bond lengths at the hydrogen-bonded site are 1.303(2) and 1.332(2) Å, respectively, whereas those of O2-N2 and C1-N2 at the opposite site are 1.272(2) and 1.367(2) Å, respectively, as shown in Table V. The twist angle around the NN plane and the phenyl ring is 37.2(1) degrees. The hydroxy group O1'-H(O1') also participates in an intermolecular hydrogen bond with the O2'-H(O2') group of the translated molecule along the *c* axis with a distance of 2.752(2) Å (Figure 3-2a, Table 3-VI). This hydrogen bond forms a one-dimensional hydrogen-bonded chain, consisting of HQNN molecules. A similar one-dimensional chain runs in parallel with inversion symmetry between the two facing molecules (Figure 3-2b). Two facing NN groups in the parallel hydrogen-bonded chain are located in proximity to each other with the NO•••ON distance of 3.159(2) Å as shown in Figure 3-2c. The situation is presumably derived from the bifurcated hydrogen bond formed by the two facing phenolic hydroxy groups and the NN groups. These two

doubly hydrogen-bonded chains are arranged in a herringbone-type structure as depicted in Figure 3-3. There are CH•••ON type contacts with the

distance of 3.11(3) Å between the methyl proton and the NO group of the adjacent molecule as shown by dashed lines.

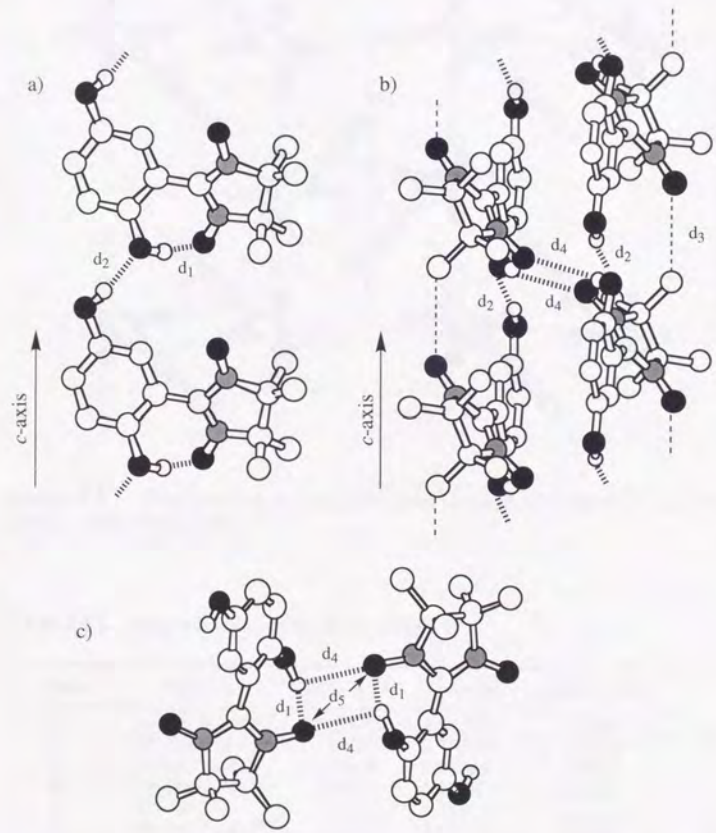


**Figure 3-2.** Crystal structure of α-HQNN: a) Hydrogen-bonded array along the c-axis. b) Facing hydrogen-bonded arrays connected by bifurcated hydrogen bonds. c) Bifurcated hydrogen-bonded pair.

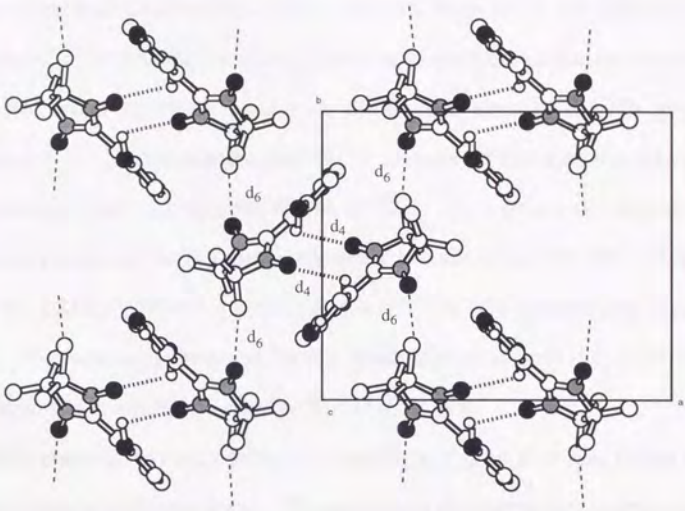


**Figure 3-3.** Projected figure along the c-axis. Dashed lines show the N-O•••H-C contact within the *ab*-plane.

**Table 3-VI.** Intermolecular distances of α-HQNN.[a]

| contact | D-H•••A | r(H•••A)/Å | r(D•••A)/Å | ∠(D-H•••A)/deg |
|---|---|---|---|---|
| $d_1$ | O1'-H(O1')•••O1 | 1.59(3) | 2.507(2) | 161(3) |
| $d_2$ | O2'-H(O2')•••O1'* | 1.87(3) | 2.752(2) | 170(1) |
| $d_3$ | C5-H(C5)•••O2* | 2.78(3) | 3.580(3) | 140(1) |
| $d_4$ | O1'-H(O1')•••O1** | 2.68(3) | 2.999(2) | 101(1) |
| $d_5$ | O1•••O1** | | 3.159(2) | |
| $d_6$ | C4-H(C4)•••O2*** | 3.11(3) | 3.679(3) | 109(1) |

[a]Symmetry code: (*) *x, y, z+1*; (**) *-x, -y, -z+1*; (***) *-x+1/2, y+1/2, -z+3/2*.

The unit cell of the β-phase crystal of HQNN contains four crystallographic equivalent molecules with a space group of $P2_1/a$ as in the case of the α-phase. The phenolic hydroxy group at 2'-position participates in the intramolecular hydrogen bond with the oxygen atom of the NN group (Figure 3-1). The intramolecular O1-O1' distance of 2.616(6) Å is slightly longer than that of α-HQNN (Table 3-VII). As a result, the degree of bond alternation in the NN group is lessened to some extent: O1-N1 1.296(4), C1-N1 1.350(5), O2-N2 1.279(5) Å, C1-N2 1.364(5), respectively (Table V). The twist angle between the NN plane and the phenyl ring is 37.2(1) degrees, and is almost the same as that of α-HQNN.

The phenolic hydroxy group at 5'-position of β-HQNN also forms the intermolecular hydrogen bond. The acceptor of the intermolecular hydrogen bond, however, is not the phenolic oxygen, but the oxygen atom of the NN group which does not participate in the intramolecular hydrogen bond (Figure 3-4a). Namely, the hydroxy group forms an intermolecular hydrogen bond with the NO group of the adjacent molecule (x+1/2, -y+5/2, z), the intermolecular O2-O2' distance being 2.777(4) Å (Table 3-VII). The hydrogen-bonded chain runs in a zigzag manner along the *a* axis. Such hydrogen-bonded chains stack along the *c* axis. The HQNN molecules in the stack are dimerized as shown in Figure 3-4b. Within the dimer, HQNN has the inversion symmetry with the molecules represented by (-x+1, -y+2, -z+1). The oxygen atom of the NN group is close to the C(1)

of the NN group (3.781(4) Å) of the molecule above, *vice versa,* shown as an overlap mode A in Figure 3-4c. On the other hand, interatomic distances of the NN groups between dimers of mode B (Figure 3-4c) are longer than 4Å.

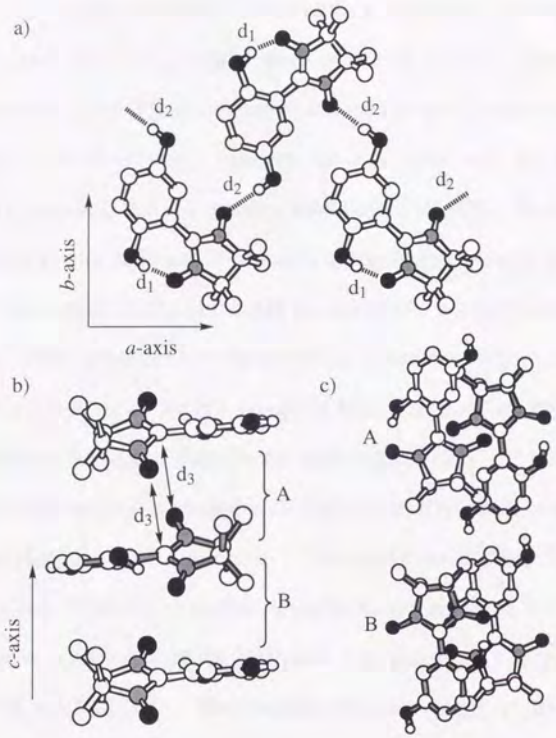


**Figure 3-4.** Crystal structure of β-HQNN: a) Hydrogen-bonded chain along the a-axis. b) Molecular stack along the c-axis. c) Two modes of overlap within the molecular stack.

**Table 3-VII.** Intermolecular distances of β-HQNN.[a]

| contact | D-H···A | r(H···A)/Å | r(D···A)/Å | ∠(D-H···A)/deg |
|---|---|---|---|---|
| $d_1$ | O1'-H(O1')···O1 | 1.73(4) | 2.616(6) | 165(4) |
| $d_2$ | O2'-H(O2')···O1* | 1.90(6) | 2.777(4) | 176(2) |
| $d_3$ | O2···C1** | ——— | 3.781(4) | ——— |

[a]Symmetry code: (*) *x+1/2, -y+5/2, z*; (**) *-x+1, -y+2, -z+1*.

In the crystal of RSNN[27], the unit cell contains four crystallographic equivalent molecules with a space group of *P2₁/n*. There is no bond alternation in the NN group due to the lack of an intramolecular hydrogen bond. The twist angle between the NN plane and the phenyl ring is 23.3(1) degrees, and it is smaller than that of HQNN. In this crystal, the hydroxy groups at 3'- and 5'-positions are hydrogen-bonded intermolecularly with the oxygen atoms of the NN groups of two adjacent molecules at both sites. They are related by the inversion symmetry (Figure 3-5a). Both of the oxygen atoms of the NN groups of RSNN, in turn, are hydrogen bonded by hydroxy groups of the adjacent molecules. Thus, the RSNN molecules are doubly hydrogen-bonded with each other, forming a hydrogen-bonded chain along the –1 0 1 direction. This hydrogen-bonded chain is slightly dimerized. While the distances of the hydrogen bonds ($d_1$ = 2.742(2) Å) are the same on one side of the molecule, they are slightly longer on the other side ($d_2$ = 2.782(2) Å). The hydrogen-bonded chains are stacked along the 1 0 1 direction (Figure 3-5b). Since the stacking is dimerized, there are two types of overlapping modes. The oxygen of the NN group ( O2 ) is located close to the C1 of the NN group of the dimeric counterpart with the intermolecular distance of 3.727(2) Å as depicted in mode A of Figure 3-5c. Since the overlap of the NN groups between the dimers (mode B) is poor, the NN groups are located remote from each other.

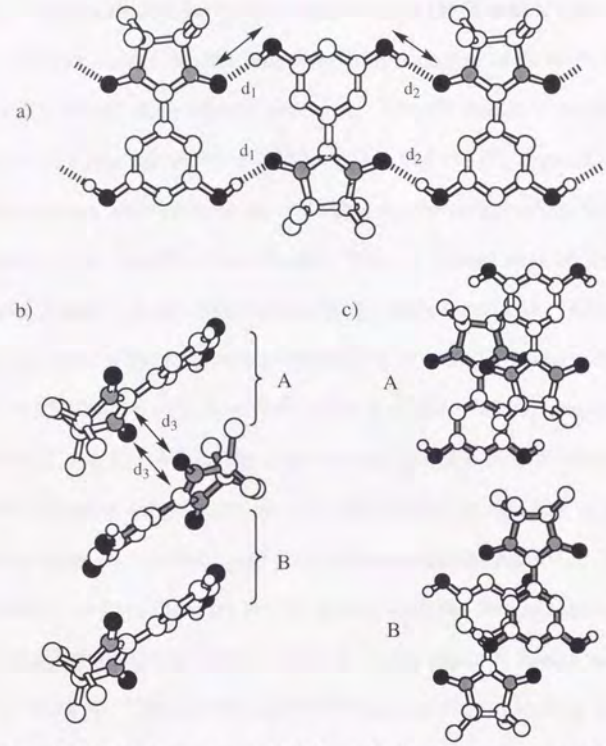


**Figure 3-5** Crystal structure of RSNN: a) Hydrogen-bonded chain along the -1 0 1 direction. b) Molecular stack along the 1 0 1 direction. c) Two modes of overlaps within the molecular stack.

**Table 3-VIII.** Intermolecular distances of RSNN.[a]

| contact | D-H···A | r(H···A)/Å | r(D···A)/Å | ∠(D-H···A)/deg |
|---|---|---|---|---|
| $d_1$ | O1'-H(O1')···O1* | 1.84(3) | 2.742(2) | 176(1) |
| $d_2$ | O3'-H(O3')···O2** | 1.89(3) | 2.782(2) | 177(1) |
| $d_3$ | O2···C1*** | ——— | 3.727(2) | ——— |

[a]Symmetry code:(*) *-x+2, -y+1, -z*; (**) *-x+1, -y+1, -z+1*, (***) *-x+1, -y+1, -z*.

### 3.3. Magnetic Property of α- HQNN, β-HQNN and RSNN

The $\chi T$ values for the polycrystalline samples of α-HQNN, β-HQNN, and RSNN are depicted in Figure 3-6. The $\chi T$ values of the three samples at room temperature were 0.383, 0.381, and 0.377, respectively. Since these values were close to the $\chi T$ value for the independent S=1/2 spin, the purity of the samples was assured. The $\chi T$ values of α-HQNN increased monotonously in the entire temperature range measured. The temperature dependence of the magnetic susceptibility of α-HQNN was well reproduced by the ST model ($J/k_b = +0.93K$) with a positive Weiss temperature of $\theta =$ +0.46 K (eq 1). While the experimental plot for β-HQNN also increased with lowering temperature, the $\chi T$ value started to decrease at temperatures lower than 3K, exhibiting an antiferromagnetic interaction. The plot was found to be best fitted by the ST model with the ferromagnetic intradimer exchange interaction of $J/k_b = +5.0$ K with a negative Weiss temperature of $\theta = -0.32$ K. The plot for RSNN[13] was also reproduced by the ST model with the ferromagnetic intradimer exchange interaction of $J/k_b = +10$ K with a negative Weiss temperature of $\theta = -4.0$ K. The magnetic parameters of all samples are summarized in Table 3-IX.

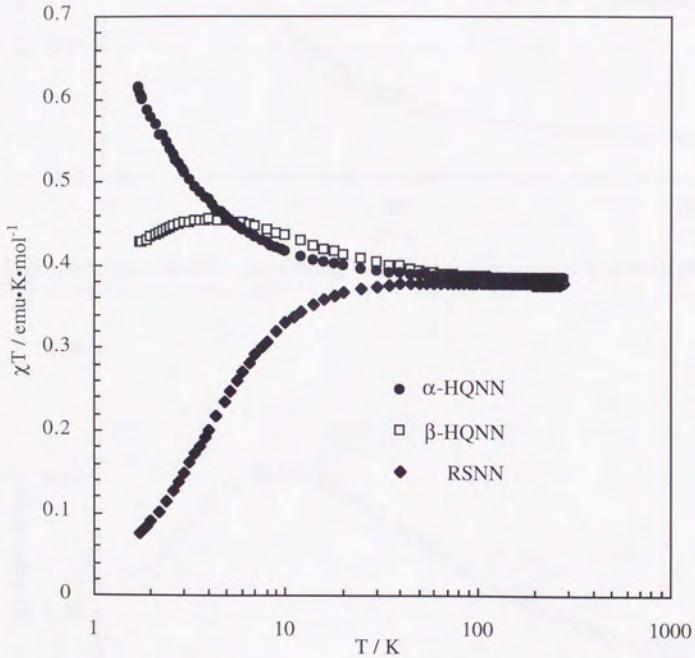


**Figure 3-6.** Temperature dependence of the magnetic susceptibility of α-HQNN, β-HQNN and RSNN.

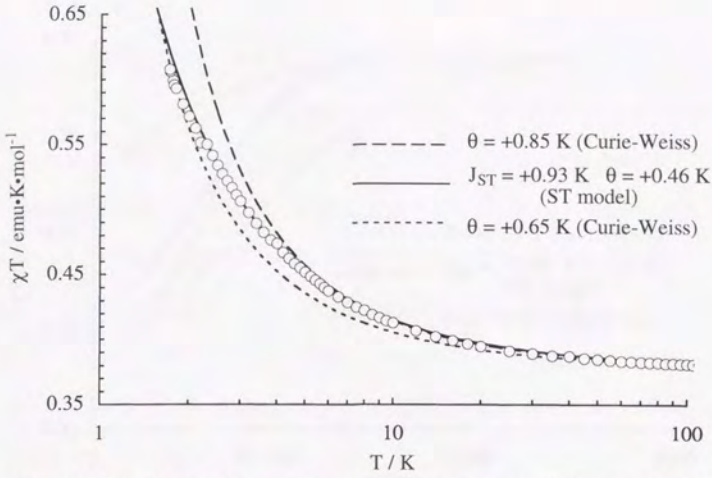


**Figure 3-7.** The theoritical curve fitting to the magnetic susceptibility of α-HQNN.

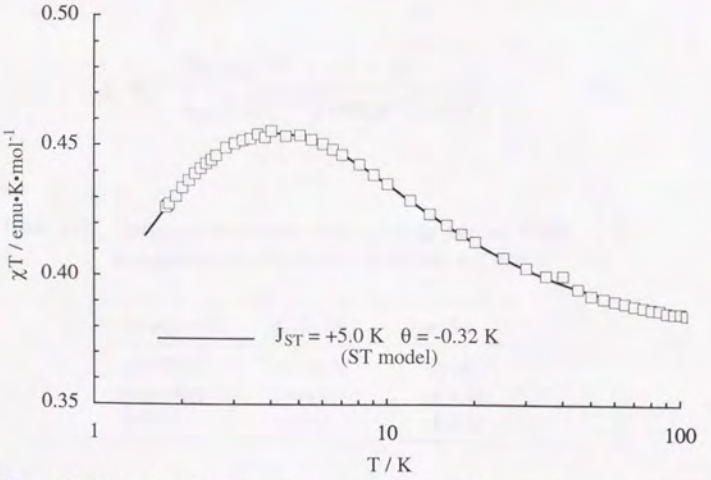


**Figure 3-8.** The theoritical curve fitting to the magnetic susceptibility of β-HQNN.

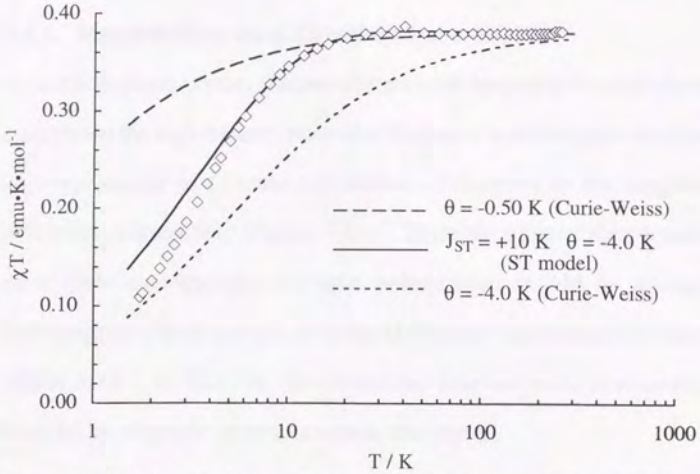


**Figure 3-9.** The theoritical curve fitting to the magnetic susceptibility of RSNN.

$$\chi = \frac{Ng^2\mu_B{}^2}{k_B(T-\theta)} \frac{1}{3+\exp(-2J/k_BT)} \qquad (1)$$

**Table 3-IX.** Exchange interaction ($J$) of a dimeric pair and Weiss temperature ($\theta$) of α-HQNN, β-HQNN, and RSNN.

| Compounds | $J_{ST}/k_B$ (K) | θ (K) |
|---|---|---|
| α-HQNN | +0.93(3) | +0.46(2) |
| β-HQNN | +5.0(1) | -0.32(1) |
| RSNN | +10(1) | -4.0(2) |

## 3.4. Discussion

### 3.4.1. Magneto-Structural Correlation of α-HQNN

In the α-phase crystal, the one-dimensional hydrogen-bonded chains are constructed through the intermolecular hydrogen bond between the phenolic hydroxy groups at C5' and C2' carbons belonging to the neighboring molecules, respectively (Figure 3-2a). Since the signs of spin densities at these sites are opposite, the spin polarization should be transmitted ferromagnetically in accord with the McConnell mechanism as shown in Figure 3-10. In fact, the intermolecular ferromagnetic interaction was detected by magnetic measurements in this crystal.

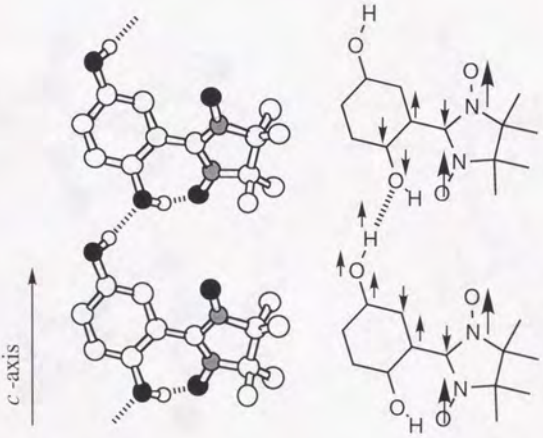


**Figure 3-10.** Plausible mechanism of transmission of spin polarization along hydrogen bond.

It is to be noted that there is a bifurcated hydrogen-bonded pair connecting the two parallel hydrogen-bonded chains. In this pair, the intermolecular distance between the oxygen atoms of the NN groups O(2(a))-O(2(b)) is as short as 3.16 Å. Although such a proximity of radicals usually causes the antiferromagnetic interaction, the experimental result suggests the presence of ferromagnetic interaction even at this site. In this respect, the ferromagnetic interaction through the hydrogen bond is considered to predominate over the antiferromagnetic through-space NO•••ON interaction (Figure 3-11).

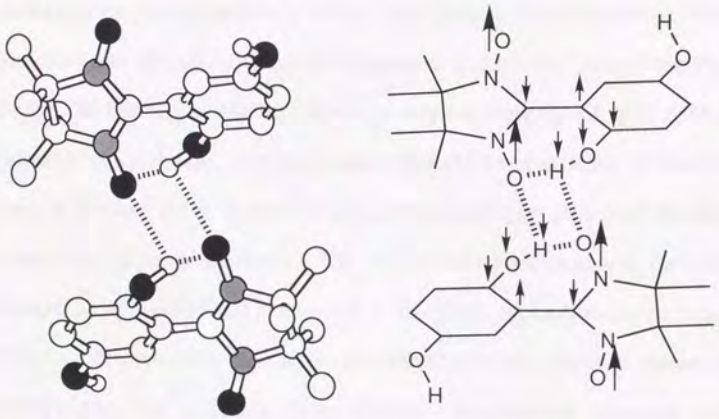


**Figure 3-11.** Plausible mechanism of transmission of spin polarization within bifurcated hydrogen-bonded pair

The presence of the ferromagnetic intermolecular interaction in this contact was reproduced through theoretical calculation by Yamaguchi *et al.*[31] When the *ortho*-hydroxy groups are removed, the model system exhibits a large antiferromagnetic intermolecular interaction due to the close contact of the NO groups. This result is strong evidence for the transmittance of ferromagnetic coupling through the hydrogen bonds.

Although one may predict the low dimensionality in the magnetic interaction for α-HQNN due to the hydrogen-bonded crystal structure, the magnetic interaction in HQNN was interpreted to be of a three-dimensional character, judged from the heat capacity data as described in the next chapter. The result suggests that the magnetic interaction along the hydrogen-bonded chain is not exceptionally strong, but comparable to other interactions. Therefore one should examine the magnetic interactions other than that through the hydrogen bonds. When the crystal structure of α-HQNN is examined more closely, one may notice that the oxygen atom of the NN group is located close to one of the methyl hydrogen atoms of the NN group of the adjacent molecule. The methyl hydrogen atoms, in fact, are found to be spin-polarized negatively.[23-26] Since the carbon atom of the methyl group, which is parallel to the π orbital of the nitronyl nitroxide moiety, has the positive spin density, presumably through the hyperconjugative mechanism, the hydrogen atoms of the methyl group are assumed to be spin-polarized negatively (Figure 3-12).

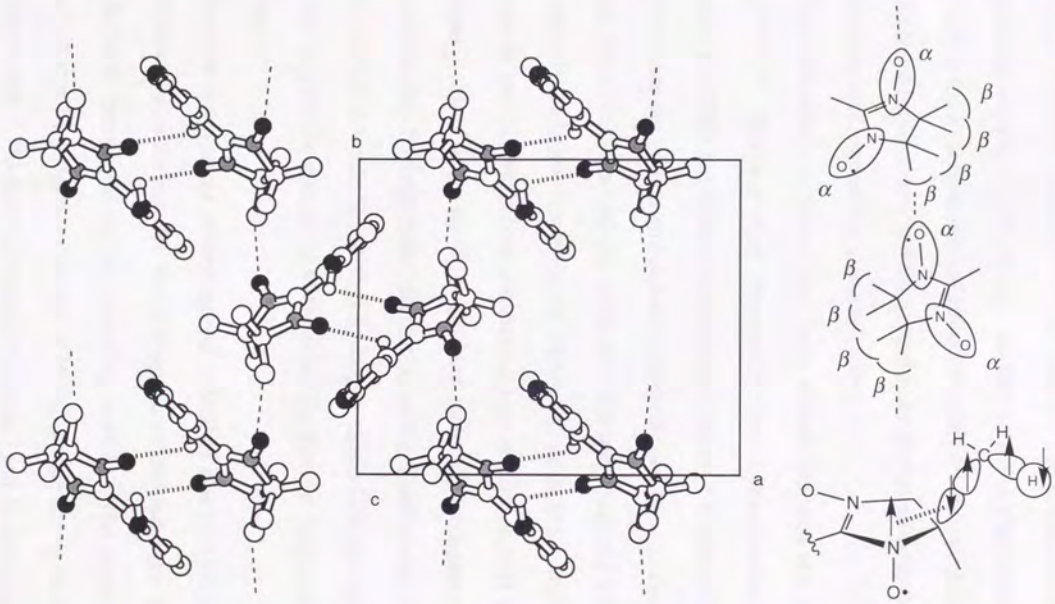


**Figure 3-12.** Ferromagnetic interaction through CH•••ON type contact

Thus, the CH•••ON interaction should increase the dimensionality of the magnetic interaction in this crystal. Incidentally, this type contact is also observed in the hydrogen-bonded chain of α-HQNN (Figure 3-2b). Such contact should cooperate with the intermolecular hydrogen bond to reinforce the ferromagnetic interaction along this chain.

This CH•••ON interaction has been already pointed out in several cases.[11,13,27,32] Veciana *et al.* discovered that *o*-hydroxyphenyl nitronyl nitroxide (*o*-HPNN) exhibits a ferromagnetic phase transition at 0.4 K.[13] *o*-HPNN does not form a one-dimensional hydrogen-bonded chain, due to the lack of an additional hydroxy group at 5'-position compared with HQNN. The three dimensional ferromagnetic interaction observed in this crystal is ascribed to the CH•••ON type interaction between the methyl group and the nitronyl nitroxide group of the adjacent molecule. Nogami *et al.* also reported that the ferromagnetic interaction in the TMPOs may be caused by the contact between the methyl hydrogen atoms having negative spin densities and the oxygen atoms of the nitroxyls having large positive spin densities.[11]

Since the temperature dependence of α-HQNN was best interpreted by the ST model with the positive Weiss temperature, the magnetic interaction may be best interpreted by the following model. The strong dimeric interaction may be assigned to the pair of HQNN connected by the bifurcated hydrogen bond. The ferromagnetically coupled pair is, then, surrounded

by neighboring pairs three-dimensionally as schematically shown in Figure 3-13. When the crystal structure is examined more closely, it is noted one pair is surrounded by 6 neighboring pairs. Two pairs are located along the hydrogen bond. The other four pairs are located in the *ab* plane through CH•••ON interactions. Such a molecular packing is consistent with the experimental data (*vide infra*).

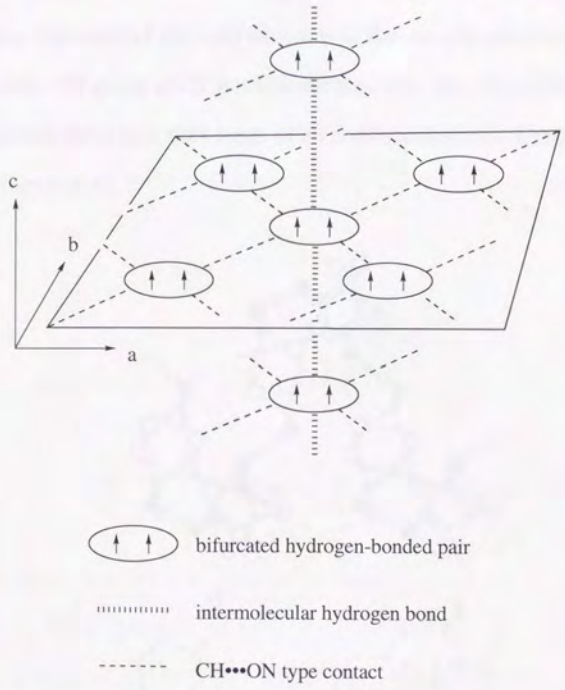


**Figure 3-13.** Schematic drawing of the spin system of α-HQNN. Ferromagnetically coupled dimeric pair surrounded by six neighboring pairs.

### 3.4.2. Magneto-Structural Correlation of β-HQNN

In β-HQNN, the oxygen atom of the NN group is hydrogen-bonded to the phenolic OH group of the adjacent molecule. It is energetically favorable that the spins at the interacting site are aligned in an antiparallel manner. Since the signs of the spin densities at the oxygen atom of the NN moiety and the OH group at C5' position are the same, the intermolecular interaction between these two sites leads to an antiferromagnetic interaction as shown in Figure 3-14.

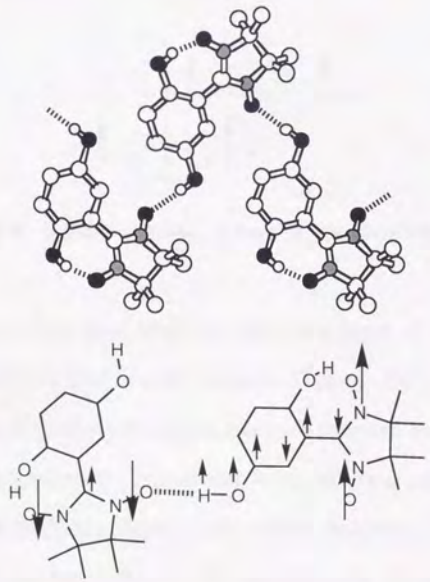


**Figure 3-14.** Plausible mechanism of antiferromagnetic interaction in β-HQNN

In fact, the antiferromagnetic interaction is detected in the low temperature region (T< 3 K). On the other hand, the magnetic interaction at the higher temperature region (T> 3 K) is ferromagnetic. This ferromagnetic interaction can not be interpreted by the coupling through the hydrogen bond but can be rationalized by the through-space π-π type interaction between the oxygen atom and the carbon atom of the NN groups of the above and below molecules, the distance between O2 and C1 being 3.78 A (overlap mode of A in Figure 3-4c).

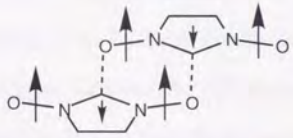

**Figure 3-15.** Schematic drawing of the π–π type interaction in β-HQNN

As these two sites have large and opposite signs of spin densities, this contact satisfies the McConnell's situation (Figure 3-15). Similar orientation in other ferromagnetic NN crystals has been reported and discussed by Rey *et al.*[33] Ferromagnetic interaction from this interaction in β-HQNN is considered to be dimeric based on the crystal structure. Thus, the structural feature is consistent with the ST model with the positive intradimer interaction, accompanied by the negative Weiss temperature.

### 3.4.3. Magneto-Structural Correlation of RSNN

Coexistence of ferro- and antiferromagnetic interaction was also recognized in the crystal of RSNN, as in the case of β-HQNN. The origin of these magnetic interactions resembles that of β-HQNN. Namely, the dimeric ferromagnetic interaction of RSNN originates from the through-space π-type interaction within the dimer along the stacking direction. The close contact is recognized between the oxygen atom of the NN group and the C1 of the NN group of the molecule underneath (mode A overlap of Figure 3-5c). On the other hand, the strong antiferromagnetic interaction is observed in RSNN. This interaction may be resulted from the double intermolecular hydrogen bonds between the hydroxy groups substituted at C(3') or C(5') positions and the oxygen atoms of the NN groups (Figure 3-5a), because the magnetic interaction through these hydrogen bonds is antiferromagnetic as described in Figure 3-16. This antiferromagnetic interaction should be enhanced significantly because of the presence of the double hydrogen bonds. One may notice that the double hydrogen-bonded pattern observed in RSNN resembles that of α-HQNN, although the nature of the intermolecular magnetic interaction is the reverse. The absolute degree of the magnetic interaction of RSNN ($|\theta|$ = 4 K), however, is much stronger than that of α-HQNN ($|J|$ = 0.95 K). The reason may be ascribed to the geometrical difference related to the double hydrogen bonds in these two crystals. In the case of α-HQNN, two NO groups are arranged in proximity

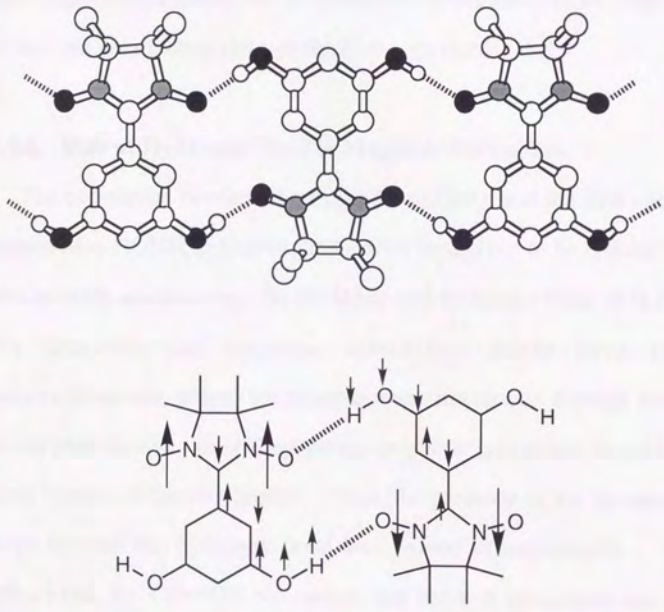


**Figure 3-16.** Plausible mechanism of antiferromagnetic interaction in RSNN

by the double bifurcated hydrogen bonds. The close contact of the NO groups in α-HQNN is considered to cancel the ferromagnetic intermolecular interaction through the hydrogen bonds. On the other hand, two NO groups in RSNN are located far apart in the double hydrogen bonds. Thus, these experimental results may be considered as evidence for the transmission of the spin polarization through the hydrogen bonds.

### 3.4.4. Role of Hydrogen Bond in Magnetic Interaction

The correlation between the magnetic property and the hydrogen bond pattern of α-HQNN, β-HQNN, and RSNN turned out to be rationalized by McConnell's mechanism. In the bifurcated hydrogen bond of α-HQNN, the intermolecular magnetic interaction might have become antiferromagnetic, unless the ferromagnetic interaction through hydrogen bonds predominates over the antiferromagnetic interaction caused by the close contact of the NO groups. Thus, the presence of the ferromagnetic route through the hydrogen bond was proved experimentally. On the other hand, the CH•••ON interaction and the π–π interaction can not be ignored. Utilization of the latter interactions, however, is difficult in the crystal engineering. On the contrary, the hydrogen bond is powerful and predictable for constructing crystal structures, and also effective in aligning electron spins intermolecularly based on the McConnell mechanism. Furthermore, hydrogen bonds can be formed between such various functional

groups as hydroxyenones, carboxy, amido, etc. Thus the hydrogen bond may be applicable widely to control the molecular arrangement of organic radicals.[34] Although the crystal design for organic ferromagnets is extremely difficult at the present stage, the hydrogen bond methodology seems to be promising in this respect.

## 3.6. Experimental

**X-ray Data Collection and Structure Determination.** The crystal structures of both phases of HQNN and RSNN were revealed by X-ray crystallography. Crystals were mounted on a Rigaku AFC-5 four-circle diffractiometer equipped with graphite-monochromatized Mo Kα radiation. The unit cell parameters were obtained by a least-square fit of the automatically centered setting from 25 reflections. In all cases, the positions of non-hydrogen atoms were obtained by direct methods using SAPI-85[35] or SHELXS-86[36] pacages. The positions of hydrogen atoms were introduced by Difference Fourier maps. Anisotropic thermal factors for all non-hydrogen atoms and isotropic thermal factors for all hydrogen atoms were applied for refinement by using UNICS-III system.[37] Atomic coordinates, bond lengths and angles, and thermal parameters were deposited at the Cambridge Crystallographic Data Center. **α-HQNN.** A bluish purple block crystal of the α-phase HQNN with dimensions of 0.32 × 0.32 × 0.28 mm was used for data collection. The intensity data was measured at ambient temperature; $\omega$ scan ( $4° < 2\theta < 55°$ ), scan speed 4° min$^{-1}$, $-19 < h < 19$, $0 < k < 16$, $0 < l < 9$. Three standard reflections (3 0 3, 6 $\bar{4}$ 0 and $\bar{4}$ $\bar{5}$ 0 ) were measured every 200 reflections and showed no significant variations throughout the data collection; 3452 reflections ($4° < 2\theta < 55°$) measured, 2204 independent reflections ($Fo > 3\sigma(Fo)$) were used for analysis ($R_{int} = 0.017$). Absorption correction was not applied. Anisotropic thermal factors for all non-hydrogen atoms and isotropic thermal factors for hydrogen atoms were used for final refinement; 240 parameters, $R = 0.051$ and $wR = 0.047$; $w = 1.0$ ($|F_o| < 20$), 0.7 ($20 \leq |F_o| < 60$), $200/|Fo|^2$ ($60 \leq |F_o|$); $S = 0.56$; max. and min. heights in final difference Fourier syntheses 0.632, -0.309 eÅ$^{-3}$; max(shift/e.s.d.) = 0.161( $y$ of H[O(2')]). **β-HQNN.** A blue needle of the β-phase HQNN with dimensions of 0.32 × 0.16 × 0.16 mm was used for analysis. The intensity data was measured at ambient temperature; $\omega$ scan ( $4° < 2\theta < 55°$ ), scan speed 4° min$^{-1}$, $-9 < h < 12$, $0 < k < 18$, $0 < l$

< 12. Three standard reflections (1 $\bar{4}$ 1, 0 0 2 and $\bar{4}$ 0 1 ) measured every 200 reflections and showed no significant variations throughout the data collection; 3330 reflections ($4° < 2\theta < 55°$) measured, 1596 independent reflections ($Fo > 3\sigma(Fo)$) were used for analysis ($R_{int} = 0.022$). Absorption correction was not applied. Anisotropic thermal factors for all non-hydrogen atoms and isotropic thermal factors for hydrogen atoms were used for final refinement; 240 parameters, $R = 0.049$ and $wR = 0.048$; $w = 1.0$ ($|F_o|<50$), $200/|Fo|^2$ ($50 \leq |F_o|$); $S = 0.73$; max. and min. heights in final difference Fourier syntheses 0.350, -0.272 eÅ$^{-3}$; max(shift/e.s.d.) = 0.223 ( $B$ of H[C(4)]1 ). **RSNN.** A blue plate crystal of RSNN with dimensions of $0.40 \times 0.36 \times 0.16$ mm was used for analysis. The intensity data was measured at ambient temperature; $\omega$ scan ( $4° < 2\theta < 55°$ ), scan speed 4° min$^{-1}$, $-10 < h < 12$, $0 < k < 25$, $0 < l < 9$. Three standard reflections (5 3 2, $\bar{2}$ $\bar{10}$ 0 and $\bar{4}$ 4 $\bar{3}$ ) measured every 200 reflections and showed no significant variations throughout the data collection; 3316 reflections ($4° < 2\theta < 55°$) measured, 2220 independent reflections ($Fo > 3\sigma(Fo)$) were used for analysis ($R_{int} = 0.025$). Absorption correction was not applied. Anisotropic thermal factors for all non-hydrogen atoms and isotropic thermal factors for hydrogen atoms were used for final refinement; 240 parameters, $R = 0.047$ and; $S = 0.58$; max. and min. heights in final difference Fourier syntheses 0.474, -0.190 eÅ$^{-3}$; max(shift/e.s.d.) = 0.044 ( $x$ of H[O(4)] ).

**Magnetic measurements.** The magnetic susceptibility of the polycrystalline samples were measured on a Quantum Design MPMS-5S SQUID susceptometer working at the field strength of 0.5 T in the temperature range of 1.8-280 K . The contribution of the sample holder and the diamagnetism of the sample were estimated from high-temperature extrapolation and then substructed to yield a paramagnetic component.

# *Chapter 4*

Magnetic Property of α-HQNN at Lower Temperature

---

## 4.1. Introduction

As described in chapter 3, three dimensional ferromagnetic intermolecular interaction was found out in the crystal of α-HQNN through magnetic measurements. In decreasing temperature, the $\chi T$ value increased monotonously for the lowest temperature end. This result suggests the possibility of a phase transition to the ferromagnet at lower temperature. Although several organic ferromagnets have been reported, they are sill rare and the crystal structure of some of organic ferromagnets have not even been available. To establish methodology for designing organic ferromagnets, the quest for a fully characterizable organic ferromagnet is inevitable. In this respect, the magnetic measurements of α-HQNN in the mK region were carried out .

## 4.2. Low temperature AC Susceptibility and Magnetization of α-HQNN

The ac susceptibility of α-HQNN increased rapidly around 0.5 K (Figure 4-1), suggesting that a phase transition to the ferromagnetic phase occurred at this temperature. Incidentally, the magnetization at temperatures lower than the transition temperature changed irregularly with lowering the temperature. In order to clarify the nature of the low temperature phase, the magnetization curve above and below $T_C$ was measured. Although the magnetization at 733 mK was dependent linearly on the external magnetic field, the magnetization curve at 80 mK exhibited a rapid saturation at 100 Oe (Figure 4-2). Since the estimated saturation value of the magnetization was very close to the theoretical value (1 $\mu_B \cdot mol^{-1}$ ), the phase transition could be regarded as a bulk-transition. It also showed a hysteretic behavior, although the coercive force was very small (less than 20 Oe). The saturation value of the magnetization curve at 409 mK was ca 70 % of the corresponding value at 80 mK. This indicates that about 30 % of the spins still fluctuate thermally at 409 mK.

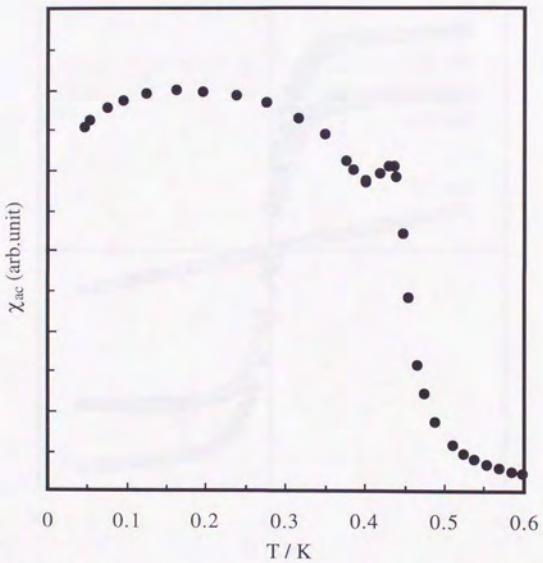


**Figure 4-1**. Ac susceptibility of α-HQNN at lower temperatures.

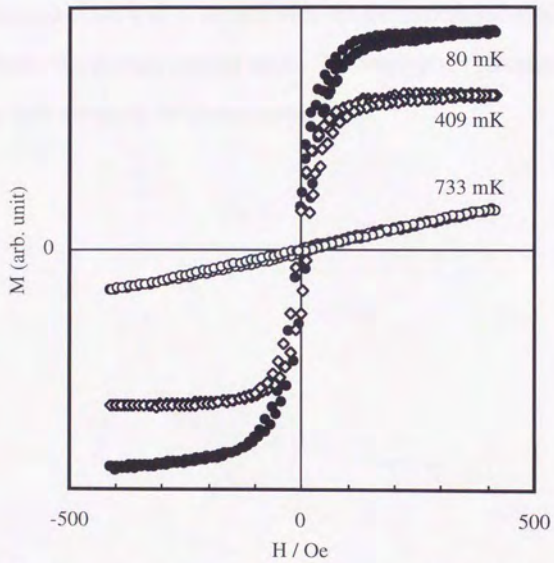


**Figure 4-2** Magnetization curves of α-HQNN measured at 733 mK, 409 mK and 80 mK

### 4.3. Heat Capacity of α-HQNN

The temperature dependence of the heat capacity, Cp, around the Tc is depicted in Figure 4-3. The heat capacity exhibited a λ-shaped anomaly with a peak at 0.42 K. The associated entropy change was evaluated to be 5.4 $J \cdot K^{-1} \cdot mol^{-1}$ by integrating the area of the peak in the Cp/T-T plot, and the obtained value was in accord with the theoretical value of $R\ln 2 = 5.76$ $J \cdot K^{-1} \cdot mol^{-1}$ within experimental error. The result gives independent evidence for the bulk nature of the phase transition.

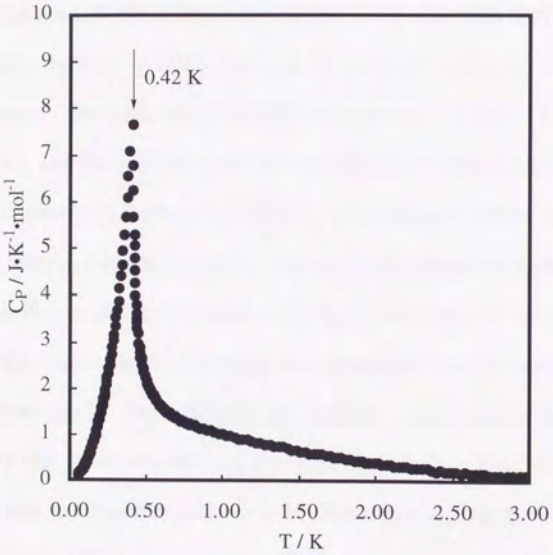


**Figure 4-3** Temperature dependence of heat capacity of α-HQNN.

### 4.4. Dimensionality of magnetic interaction of α-HQNN

Dimensionality of the magnetic interaction is closely related to the mechanism of the spin ordering as shown in Figure 4-4. In α-HQNN, the anomaly in the heat capacity is observed at 0.42 K (Figure 4-3). The ratio of $T_C$ and θ is known to reflect the dimensionality of the spin interaction.[38] While the ratio ($T_C/\theta$) is equal to 1 in the molecular field approximation, it decreases together with a decrease in dimensionality of the spin-spin interaction. The ratio for α-HQNN is estimated to be 0.51 ($T_C$ = 0.42 K, θ = 0.82 K), and the value is close to that of the three-dimensional Heisenberg model as shown in Table 4-I (Tc/θ = 0.56 for a simple cubic lattice).

The relative ratio of the entropy in the lower temperature region than Tc ($S_C$) and that in the higher region ($S_\infty - S_C$) is evaluated to be 0.60 to 0.40. Since the ratio should increase accompanied by the decrease in the dimensionality of the spin-spin interaction, it also serves as a scale to estimate the dimensionality of the spin system.[38] The obtained value suggest that the dimensionality of α-HQNN is close to the three-dimensional Heisenberg model (z=6) as shown in Table 4-I. These results also substantiate the picture of the spin system discussed previously.

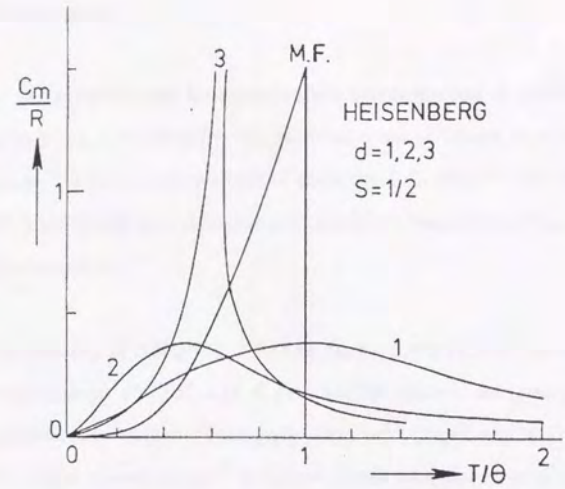


**Figure 4-4.** Temperature dependence of heat capacity in the model spin system.[38]

**Table 4-I.** The ratio of $T_C/\theta$ and the entropy of the spin system($S_C$) in the lower temperature region than $T_C$ and that ($S_\infty$-$S_C$) in the higher temperature region than $T_C$.

| Model or crystal | $T_C/\theta$ | $S_C$(%) | $S_\infty$-$S_C$(%) |
|---|---|---|---|
| Mean field | 1 | 100 | 0 |
| Ising s.c. (Z=6) | 0.75 | 81 | 19 |
| Ising diamond (Z=4) | 0.67 | 74 | 26 |
| Heisenberg f.c.c | 0.67 | 67 | 33 |
| Heisenberg b.c.c | 0.63 | 65 | 35 |
| Heisenberg s.c. | 0.56 | 62 | 38 |
| **α-HQNN** | **0.56** | **60** | **40** |

$S_C$: Entropy change between 0 K and $T_C$.
$S_\infty$: Entropy change of phase transition.

## 4.5. Experimental

**AC susceptibility and low-temperature magnetization of α-HQNN.** The ac susceptibility ($\chi_{ac}$) of α-HQNN was measured down to 40 mK in a $^3$He-$^4$He dilution refrigerator[39] at the ac magnetic field of about 10 μT (127Hz).[40] The magnetization at 80, 409, and 733 mK were measured with a standard integration method similar to that described previously.[41]

**Heat capacity of α-HQNN.** The heat capacity of α-HQNN was measured in the temperature range of 0.057-3.28 K in a $^3$He-$^4$He dilution refrigerator with a usual adiabatic heat pulse method. The sample holder was charged with 19.7 mg of α-HQNN and 25.1 mg of Apiezon grease. In order to obtain information on the spin ordering, it is necessary to exclude the phonon contribution from the measured heat capacity data. Since the heat capacity derived from lattice at cryogenic temperatures is proportioned to $T^3$ according to Debye's approximation, the lattice heat capacity is estimated from the slope of the Cp-$T^3$ plot. The pure contribution of the spin system was obtained, after substracting the contribution of the phonon from the overall heat capacity.

# *Chapter 5*

Isotope Effect on the structure and the magnetic property of HQNN and RSNN

---

## 5.1. Introduction

The author has descrived the ferromagnetic phase transition at 0.5 K of α-phase crystal of HQNN (2,5-dihydroxyphenyl nitronyl nitroxide), which is a stable organic radical carrying hydroxy groups as orientation controlling sites in crystal. Recently, Veciana et al. reported the ferromagnetic phase transition (0.45K) of *o*-hydroxyphenyl nitronyl nitroxide.[13] These results suggest that the hydrogen bond is able to systematize open-shell molecules into a molecular assembly of prominent magnetic properties. Replacement of hydrogen of the hydroxy group with deuterium in such organic radicals should perturb the crystal structures and intermolecular magnetic interactions. In this respect, the author has investigated the crystal structure and magnetic property of the α-HQNN-$d_2$, β-HQNN-$d_2$, and RSNN-$d_2$ in which phenolic hydrogens are substituted with deuterium.

## 5.2. Preparation of Deuterated α-HQNN, β-HQNN and RSNN

Deuterated α-HQNN, β-HQNN and RSNN were prepared by recrystallization from ethanol-$d_1$. The α- and β-phase crystals of HQNN were obtained by using small amount of corresponding seed crystals.[42]

In α-HQNN-$d_2$, the IR spectrum of the crystal showed peaks at 2434 which were assignable to the hydrogen-bonded O-D stretching. Besides, a broad peak was observed at 1800-2100 $cm^{-1}$ assignable to the hydrogen-bonded O-D stretching of the intramolecular hydrogen bond. The results suggests that both intra- and intermolecular hydrogen bonds were deuterated (Figure 5-1). The OD stretching bands of β-HQNN-$d_2$ appeared also at 2473 $cm^{-1}$ and in the range of 2300-1900 $cm^{-1}$, assignable to the intermolecular and intramolecular hydrogen bonds, respectively. In the case of RSNN-$d_2$, four peaks were observed at 2540, 2466, 2391, and 2349 $cm^{-1}$.

The percentage of deuteration of α-HQNN was estimated to be more than 70 % based on the intensities of IR absorption peaks. The ratio of deuteration of β-HQNN and RSNN were also estimated to be more than 80 % and 60 %, respectively.

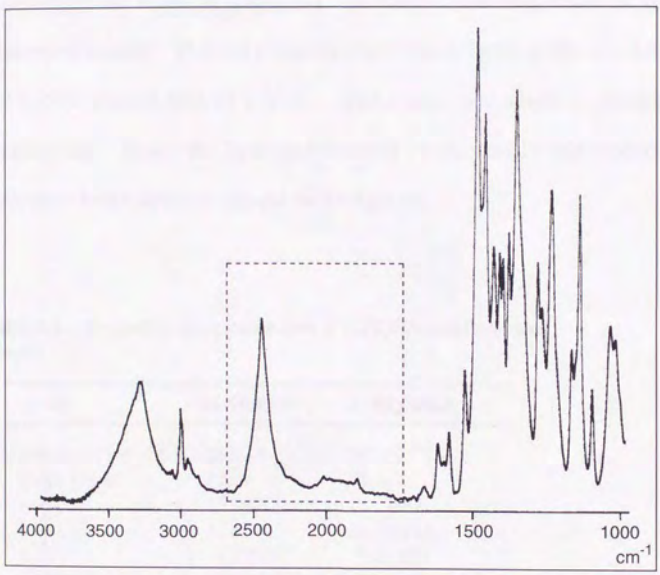


**Figure 5-1.** IR spectrum of α-HQNN-$d_2$ (70%). Enclosed peaks with dashed frame are assigned to the O-D stretching.

### 5.3. Crystallographic Features of the Deuterated α-HQNN

Crystal structure of deuterated α-HQNN was also characterized by X-ray crystallography. Because of incomplete deuteration, the reflection peaks were broader than non-deuterated sample. Crystallographic parameters are listed in Table 5-I, in comparison with those of the non-deuterated sample. The cell parameters are almost same as the non-deuterated α-HQNN, except that of c-axis. The c-axis was slightly elongated by deuteration. Since the hydrogen-bonded chain runs in this direction, the hydrogen bond distance should be elongated.

**Table 5-I.** Crystallographic parameters of α-HQNN and deuterated sample.

| crystal | α–HQNN | α–HQNN-$d_2$ |
|---|---|---|
| molecular weight | 265.29 | 267.29 |
| space group | $P2_1/n$ | $P2_1/n$ |
| $a$, Å | 15.142(3) | 15.138(2) |
| $b$, Å | 12.320(1) | 12.336(3) |
| $c$, Å | 7.196(1) | 7.211(3) |
| $\beta$, deg | 99.18(2) | 99.19(2) |
| $V$, Å$^3$ | 1325.3(4) | 1329.2(6) |
| $Z$ | 4 | 4 |
| $T$, °C | 25 | 25 |
| $\rho$, g cm$^{-1}$ | 1.331 | 1.337 |
| Reflections | 2204 | 1501 |
| Parameters | 240 | 240 |
| $R$ | 0.051 | 0.071 |
| $R_W$ | 0.047[a] | —— |

a) $W = 1.0$ ($|F_o|<20$), $0.7$ ($20 \le |F_o| < 60$), $200/|Fo|^2$ ($60 \le |F_o|$)

**Table 5-II.** Positional parameters and equivalent isotropic thermal parameters of deuterated α-HQNN.

| atom | *x* | *y* | *z* | *B*eq (Å$^2$) |
|---|---|---|---|---|
| O1' | 0.0629 (5) | 0.8336 (3) | 0.5629 (3) | 3.3 (1) |
| O2' | 0.7515 (5) | 0.7282 (4) | 0.4716 (3) | 4.3 (1) |
| O1 | 0.1065 (5) | 1.0330 (3) | 0.5954 (3) | 4.2 (1) |
| O2 | 0.6616 (5) | 0.8965 (3) | 0.7531 (3) | 4.2 (1) |
| N1 | 0.2508 (6) | 1.0165 (4) | 0.6581 (3) | 3.0 (1) |
| N2 | 0.5158 (6) | 0.9558 (4) | 0.7307 (3) | 2.7 (1) |
| C2' | 0.2352 (7) | 0.8159 (4) | 0.5391 (3) | 2.6 (1) |
| C3' | 0.2492 (7) | 0.7388 (4) | 0.4744 (4) | 3.0 (1) |
| C4' | 0.4222 (8) | 0.7097 (4) | 0.4538 (3) | 3.2 (1) |
| C5' | 0.5850 (7) | 0.7594 (4) | 0.4965 (3) | 2.7 (1) |
| C6' | 0.5743 (7) | 0.8380 (4) | 0.5602 (3) | 2.8 (1) |
| C1' | 0.3975 (7) | 0.8673 (4) | 0.5828 (3) | 2.3 (1) |
| C1 | 0.3873 (6) | 0.9447 (4) | 0.6542 (3) | 2.4 (1) |
| C2 | 0.2619 (8) | 1.0685 (4) | 0.7482 (4) | 3.1 (1) |
| C3 | 0.4741 (7) | 1.0536 (4) | 0.7843 (3) | 2.8 (1) |
| C4 | 0.1957 (9) | 1.1858 (5) | 0.7358 (4) | 4.5 (2) |
| C5 | 0.1315 (9) | 1.0026 (6) | 0.7986 (5) | 4.9 (2) |
| C6 | 0.5978 (9) | 1.1449 (5) | 0.7591 (5) | 4.8 (2) |
| C7 | 0.5168 (10) | 1.0262 (6) | 0.8837 (4) | 4.8 (2) |
| H(O1') | 0.050 (7) | 0.905 (4) | 0.571 (3) | 3.0 (11) |
| H(O2') | 0.833 (8) | 0.759 (5) | 0.493 (4) | 5.2 (15) |
| H(C3') | 0.148 (8) | 0.702 (5) | 0.443 (4) | 6.0 (16) |
| H(C4') | 0.432 (6) | 0.660 (3) | 0.411 (3) | 1.7 (9) |
| H(C6') | 0.690 (7) | 0.877 (4) | 0.593 (3) | 3.8 (13) |
| H(C4)1 | 0.217 (7) | 1.217 (5) | 0.789 (4) | 4.6 (14) |
| H(C4)2 | 0.269 (9) | 1.228 (6) | 0.692 (4) | 6.9 (18) |
| H(C4)3 | 0.065 (9) | 1.184 (5) | 0.717 (4) | 6.3 (17) |
| H(C5)1 | 0.126 (9) | 1.043 (6) | 0.854 (4) | 7.7 (19) |
| H(C5)2 | 0.015 (8) | 0.998 (5) | 0.758 (4) | 6.0 (16) |
| H(C5)3 | 0.190 (8) | 0.927 (5) | 0.815 (4) | 5.7 (16) |
| H(C6)1 | 0.568 (7) | 1.206 (4) | 0.789 (3) | 3.6 (12) |
| H(C6)2 | 0.576 (10) | 1.157 (6) | 0.689 (5) | 7.6 (19) |
| H(C6)3 | 0.724 (10) | 1.126 (6) | 0.777 (5) | 8.7 (22) |
| H(C7)1 | 0.491 (8) | 1.087 (5) | 0.916 (4) | 5.4 (15) |
| H(C7)2 | 0.646 (9) | 1.016 (6) | 0.902 (5) | 7.4 (19) |
| H(C7)3 | 0.452 (11) | 0.959 (7) | 0.899 (5) | 10.4 (24) |

The molecular structure of the deuterated α-HQNN is almost same as the non-deuterated sample without hydroxy groups. The bond distances of the deuterated α-HQNN are shown in Table 5-III, in comparison with those of non-deuterated sample. The bond lengths of the O-D bonds are shortened in comparison with O-H. The dihedral angle between the benzene ring and the NN plane is 37.0(1) degrees, and it is also similer to the non-deuterated sample.

The intermolecular distances of the deuterated sample is shown in Table 5-IV, in comparison with those of non-deuterated sample. Reflecting the shortened O-D bond lengths, hydrogen bond distances are varied by deuteration. The intramolecular hydrogen bond distances are 2.518(6) Å (O•••O) and 1.66(5) Å (O•••D) and they are longer than those of the non-deuterated sample. The intermolecular hydrogen bond along the hydrogen-bonded chain ( c-axis) is also elongated by deuteration. The interatomic distances are 2.765(6) Å (O•••O) and 2.03(6) Å (O•••D), respectively. However, the interatomic distances in the bifurcated hydrogen bonding region are almost same in comparison with those of non-deuterated sample.

Although the quality of this X-ray analysis is not very good, it seems to be significant, because only the bond distances related to the hydroxy groups are varied, while other bond lengths are not changed.

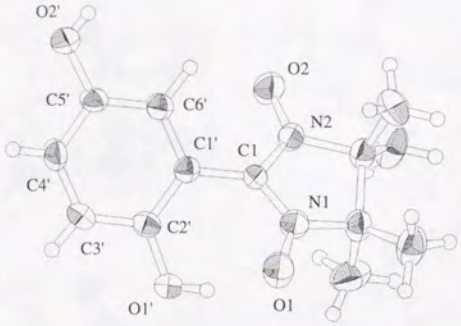


**Figure 5-2.** ORTEP drawing (50% probability) of α-HQNN-$d_2$ with atomic numbering scheme.

**Table 5-III.** Selected bond lengths (Å) of α-HQNN and α-HQNN-$d_2$.

| Bonds | **α-HQNN** | **α-HQNN-$d_2$** |
|---|---|---|
| O1-N1 | 1.303(2) | 1.308(6) |
| O2-N2 | 1.272(2) | 1.281(6) |
| C1-N1 | 1.332(2) | 1.332(7) |
| C1-N2 | 1.367(2) | 1.369(7) |
| C1-C1' | 1.457(3) | 1.453(7) |
| C1'-C2' | 1.400(3) | 1.400(7) |
| C2'-C3' | 1.388(3) | 1.381(8) |
| C3'-C4' | 1.378(3) | 1.381(8) |
| C4'-C5' | 1.392(3) | 1.389(8) |
| C5'-C6' | 1.380(3) | 1.379(8) |
| O1'-C2' | 1.367(2) | 1.365(6) |
| O2'-C5' | 1.370(3) | 1.370(7) |
| O1'-H(O1') | 0.95(3) | 0.90(5) |
| O2'-H(O2') | 0.89(3) | 0.74(6) |

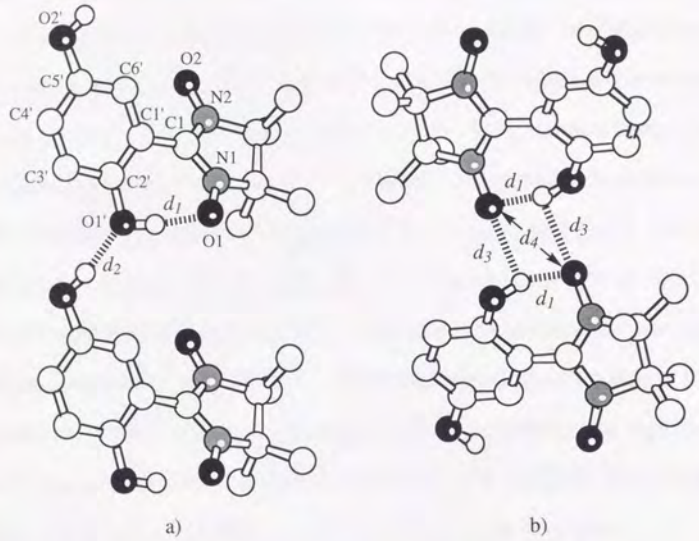


**Figure 5-3.** Crystal structure with distance code of α-HQNN: a) Hydrogen-bonded chain along c-axis b) Bifurcated hydrogen-bonded pair.

**Table 5-IV.** Intermolecular distances of α-HQNN and α-HQNN-$d_2$

| | | α-HQNN | | α-HQNN-$d_2$ | |
|---|---|---|---|---|---|
| contact | D-H···A | r(H···A)/Å | r(D···A)/Å | r(H···A)/Å | r(D···A)/Å |
| $d_1$ | O1'-H(O1')···O1 | 1.59(3) | 2.507(2) | 1.66(5) | 2.518(6) |
| $d_2$ | O2'-H(O2')···O1'* | 1.87(3) | 2.752(2) | 2.03(6) | 2.765(6) |
| $d_4$ | O1'-H(O1')···O1** | 2.68(3) | 2.999(2) | 2.70(5) | 3.002(6) |
| $d_5$ | O1···O1** | ——— | 3.159(2) | ——— | 3.154(6) |

[a]Symmetry code: (*) *x, y, z+1*; (**) *-x, -y, -z+1*; (***) *-x+1/2, y+1/2, -z+3/2*.

## 5.4. Magnetic Property of Deuterated α-HQNN, β-HQNN and RSNN

The magnetic susceptibility of the deuterated samples were measured at the temperature range of 1.8–280 K, using a SQUID magnetometer (main field 5 kOe). The $\chi T$ value of these samples at an ambient temperature assures the purity of the samples. When the temperature dependence of the magnetic susceptibility of α-HQNN-$d_2$ was compared with the non-deuterated sample, the $\chi T$ value at 1.8 K was decreased from 0.600 to 0.570 emu•K•$mol^{-1}$ (Figure 5-4). The effect of deuteration was more pronounced in the case of RSNN. Upon deuteration, the $\chi T$ value at 1.8 K increased from 0.078 to 0.280 emu•K•$mol^{-1}$, indicating the significant decrease in the antiferromagnetic interaction. In β-HQNN, the effect of deuteration on the magnetic interaction is found to be negligible.

The temperature dependence of the heat capacity of the 70 % deuterated α-HQNN-$d_2$ showed a broad λ-shaped anomaly in the temperature range of 0.38-0.40 K (Figure 5-5). The peak position was shifted to the lower temperature side compared with the non-deuterated sample.

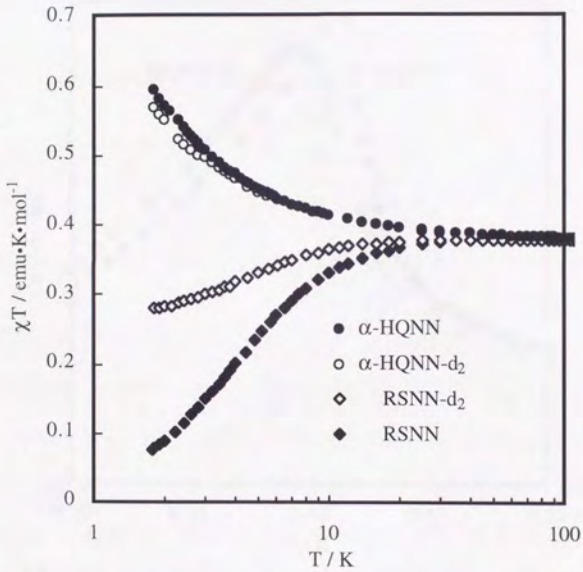


**Figure 5-4.** Magnetic susceptibility of the deuterated samples of α-HQNN and RSNN together with the data of non-deuterated samples.

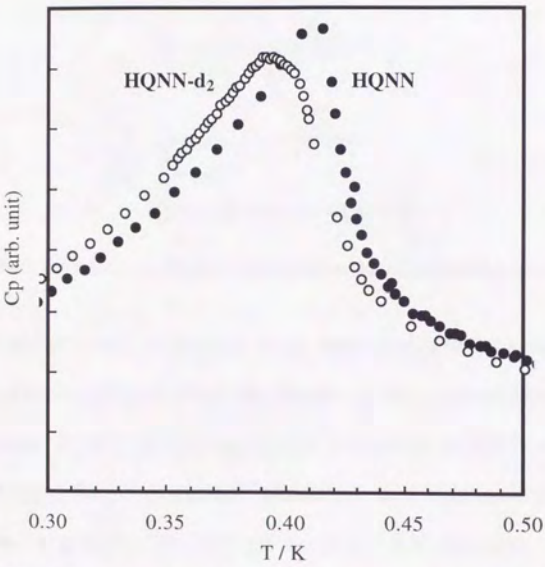


**Figure 5-5.** Temperature dependence of heat capacity of deuterated α-HQNN.

## 5.5. Discussion

Generally, the H-X bond distance is shortened by substituting hydrogen with deuterium. In the case of a hydrogen bond, the shortening of the O-D bond causes an elongation of the hydrogen bond distances as shown in Figure 5-6.[43]

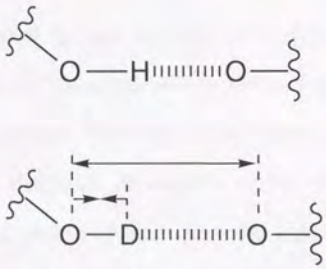


**Figure 5-6.** Schematic drawing of the isotope effect on the hydrogen bond.

If the hydrogen bond contributes to the transmission of the spin-polarization, the deuteration should affect the degree of the intermolecular magnetic interaction. In fact, the hydrogen bond distance of α-HQNN was elongated and the apparent ferromagnetic interaction decreased upon deuteration of the hydroxy groups. Namely, $\chi T$ value at 1.8 K decreases by 5 % (from 0.60 to 0.57 emu•K•mol$^{-1}$) for the 70 % deuterated sample.

In β-HQNN, the effect of deuteration on the magnetic interaction is found to be negligible. Since the through-space interaction predominates over the interdimer interaction through the hydrogen bond, the result is not in consistent with the above interpretation.

The effect of deuteration on RSNN is much more pronounced than that on α-HQNN. The magnetic susceptibility increases by 350 % at (from 0.08 to 0.28 emu•K•mol$^{-1}$) at 1.8 K for the 60 % deuterated sample. This may be reasonable, because the hydrogen bonds in RSNN are stronger and doubly-formed.

The maximum of the heat capacity of α-HQNN was sifted to the lower temperature side and the peak was broadened compared with that of the hydrogen counterpart. The shift to the lower temperature indicates the decrease in the magnetic interaction of the deuterated sample. The broadening of the peak may arise from the inhomogeneous distribution of the deuterated hydroxy groups due to the incomplete deuteration.

Although the detailed discussion on the isotope effect should await the result of the completely deuterated samples, the change of the magnetic interactions in these crystals (α-HQNN, β-HQNN, RSNN) is consistent with the interpretation that the magnetic interaction is transmitted through the hydrogen bond.

## 5.6. Experimental

**X-ray Data Collection and Structure Determination of α-HQNN.** The crystal structure of α-HQNN-d2 was revealed by X-ray crystallography. Crystal was mounted on a Rigaku AFC-5 four-circle diffractiometer equipped with graphite-monochromatized Mo Kα radiation. The unit cell parameters were obtained by a least-square fit of the automatically centered setting from 25 reflections. The positions of non-hydrogen atoms were obtained by direct methods using SHELXS-86[36] package. The positions of hydrogen atoms were introduced by difference fourier maps. Anisotropic thermal factors for all non-hydrogen atoms and isotropic thermal factors for all hydrogen atoms were applied for refinement by using UNICS-III system.[37] **α-HQNN-$d_2$.** A bluish purple block crystal of the α-HQNN-$d_2$ with dimensions of 0.30 × 0.30 × 0.30 mm was used for data collection. The intensity data was measured at ambient temperature; $\omega$ scan ( $5° < 2\theta < 55°$ ), scan speed 4° $min^{-1}$, $-20 < h < 20$, $0 < k < 16$, $0 < l < 9$. Three standard reflections ($\bar{2}\,\bar{1}\,1$, $\bar{4}\,0\,0$ and $3\,\bar{2}\,0$ ) were measured every 150 reflections and showed no significant variations throughout the data collection; 3536 reflections ($4° < 2\theta < 55°$) measured, 1501 independent reflections ($Fo > 3\sigma(Fo)$) were used for analysis ($R_{int} = 0.036$). Absorption correction was not applied. Anisotropic thermal factors for all non-hydrogen atoms and isotropic thermal factors for hydrogen atoms were used for final refinement; 240 parameters, $R = 0.071$; $S = 1.42$; max. and min. heights in final difference Fourier syntheses 0.332, -0.301 $eÅ^{-3}$; max(shift/e.s.d.) = 0.056( $B$of H[O(2')]).

**Heat capacity of α-HQNN-$d_2$.** The heat capacity of α-HQNN-$d_2$ was measured in the temperature range of 0.056-4.35 K in a $^3$He-$^4$He dilution refrigerator with a usual adiabatic heat pulse method. The sample holder was charged with 2.646 mg of α-HQNN-$d_2$ and 5.754 mg of Apiezon grease. The lattice contribution were corrected as in the case of α-HQNN.

# *Chapter 6*

## Concluding Remarks

Nitronyl nitroxide derivatives carrying a hydroquinone or a resorcinol moiety (**HQNN**, **RSNN**) were designed and prepared to form hydrogen bonded crystals. In all cases, the magnetic behaviors are consistent with McConnell's theory, when the spin densities at the interacting sites through hydrogen bonds are taken into account. Among them, α-**HQNN** turned out to exhibit a ferromagnetic phase transition at 0.5 K and it is a first organic ferromagnet which is constructed by hydrogen bonds. In order to connect the spin polarized sites more decisively in an appropriate mode, it may be effective to utilize hydrogen-bonds at multi-sites. The utilization of hydrogen bonds may also be effective in controlling the magnetic property through the switching of hydrogen bonds.[44] Although it is crucial to induce significant spin densities on the hydrogen-bonding sites, the hydrogen bond may be utilized as the "spin coupler". Thus it may play an important role in designing various artificial spin systems[1].

As an extension of the current study, this system has the following potentialities. First, hydroquinone, which plays an important role in HQNN, is supposed to form a quinhydrone complex, when it is mixed with quinone. In the complex, charge transfer interaction is coupled with hydrogen bond, exhibiting an intriguing properties, such as a pressure-induced phase transition, etc.[45] Although a quinhydrone complex has not been obtained between HQNN and BQNN[46], which is obtained by the oxidation of the former. Formation of quinhydron with HQNN, however, may become possible by an expansion of the π-system of the quinone skeleton of BQNN.

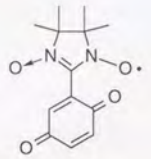

**BQNN**

Second, some hydroquinone derivatives are known to exhibit a structural phase transition under photo-irradiation or application of the external pressure. In fact, a preliminary result on the pressure dependence of the frequency of the OH stretching frequency in IR spectrum exhibits an abrupt softening at external pressures higher than 1 G Pa. Since a spin source is introduced into the hydroquinone moiety, this system may exhibit a switching of the magnetic properties upon the application of the external-pressure.

Such an external-field dependence of magnetic properties is considered to be an advantage of organic spin systems. After all, this current research should shed light upon these intriguing potentialities.

# References


1) For a recent overview, see: a) Miller, J. S.; Dougherty, D. A., Eds. *Mol. Cryst. Liq. Cryst.*, **1989**, *176*, 1-562. b) *Advanced Organic Solid State Materials*; Chiang, L. Y.; Chaikin, P. M.; Cowan, D. O., Eds.; Materials Research Society: Pittsburgh, PA, **1989**; pp 3-92. c) *Molecular Magnetic Materials*; Gatteschi, D.; Kahn, O.; Miller, J. S.; Palacio, F., Eds.; Kiuwer Academic: Dordrecht, **1991**; Vol. A198. d) Iwamura, H.; Miller, J. S. Eds., *Mol. Cryst. Liq. Cryst.*, **1993**, *232/233*, 1-360/1-366. e) Iwamura, H. *Adv. Phys. Org. Chem.*, **1990**, *26*, 179. f) Kollmar, C.; Kahn, O. *Acc. Chem. Res.*, **1993**, *26*, 259. g) Miller, J. S.; Epstein, A. J. *Angew. Chem., Int. Ed. Engl.*, **1994**, *33*, 385. h) Rajca, A. *Chem. Rev.*, **1994**, *94*, 871-893. i) Miller, J. S.; Epstein, A. J., Eds., *Mol. Cryst. Liq. Cryst.*, **1995**, *272-274*. j) Izuoka, A.; Kumai, R.; Sugawara, T. *Adv. Mater.*, **1995**, *7*, 672.

2) a) Itoh, K. *Chem. Phys. Lett.*, **1967**, *1*, 235. b) Wasserman, E.; Murray, R. W.; Yanger, W. A.; Trozzolo, A. M.; Smolinsky, G. *J. Am. Chem. Soc.*, **1967**, *89*, 5076.

3) a) Longuet-Higgins, H. C.; Pople, A. J. *Proc. Phys. Soc. (London)*, **1955**, *A68*, 591. b) Mataga, N. *Theor. Chim. Acta*, **1968**, *10*, 372. c) Ovchinnikov, A. A. *Theoret, Chim. Acta*, **1980**, *47*, 297.

4) a) Sugawara, T.; Bandow, S.; Kimura, K.; Iwamura, H.; Itoh, K. *J. Am. Chem. Soc.*, **1984**, *106*, 6449. b) Sugawara, T.; Bandow, S.; Kimura, K.; Iwamura, H.; Itoh, K. *J. Am. Chem. Soc.*, **1986**, *108*, 368.

5) a) Murray, M. M.; Kaszynski, P.; Kaisaki, D. A.; Chang, W.; Dougherty, D. A. *J. Am. Chem. Soc.*, **1994**, *116*, 8152. b) Nishide, H.; Kaneko, T.; Nii, T; Katoh, K; Tsuchida, E.; Lahti, P. M. *J. Am. Chem. Soc.*, **1996**, *118*, 9695. c) Rajca, A.; Utamapanya, S. *J. Am. Chem. Soc.*, **1993**, *115*. 10688.

6) a) Teki, Y.; Fujita, I.; Takui, T.; Kinoshita, T.; Itoh, K. *J. Am. Chem. Soc.*, **1994**, *116*, 11499-11505. b) Matsuda, K.; Nakamura, N.; Inoue, K.; Koga, N.; Iwamura, H. *Bull. Chem. Soc. Jpn.*, **1996**, *69*, 1483.

7) a) Mukai, K.; Nishiguchi, H.; Deguchi, Y.; *J. Phys. Soc. Jpn.*, **1967**, *23*, 125. b) Mukai, K. *Bull. Chem. Soc. Jpn.*, **1969**, *42*, 40.

8) Sugawara, T.; Murata, S.; Kimura, K.; Iwamura, H. *J. Am. Chem. Soc.*, **1985**, *107*, 5293.

9) a) Kinoshita, M.; Turek, P.; Tamura, M.; Nozawa, K.; Shiomi, D.; Nakazawa, Y.; Ishikawa, M.; Takahashi, M.; Awaga, K.; Inabe, T.; Maruyama, Y. *Chem. Lett.*, **1991**, 1225. b) Nakazawa, Y.; Tamura, M.; Shirakawa, N.; Shiomi, D.; Takahashi, M.; Kinoshita, M.; Ishikawa, M. *Phys. Rev. B: Condens. Matter.*, **1992**, *46*, 8906.

10) Chiarelli, R.; Novak, M. A.; Rassat, A.; Tholence, J. L. *Nature*, **1993**, *363*, 147.

11) Nogami, T.; Ishida, T.; Tsuboi, H.; Yoshikawa, H.; Yamamoto, H.; Yasui, M.; Iwasaki, F.; Iwamura, H.; Takeda, N.; Ishikawa, M. *Chem. Lett.*, **1995**, 635-636. and references therein.

12) Sugawara, T.; Matsushita, M. M.; Izuoka, A.; Wada, N.; Takeda, N.; Ishikawa, M. *J. Chem. Soc., Chem. Commun.*, **1994**, 1723.

13) Cirujeda, J.; Mas, M.; Molins, E.; Panthou, F. L.; Laugier, J.; Park, J. G.; Paulsen, C.; Rey, P.; Rovira, C.; Veciana, J. *J. Chem. Soc., Chem. Commun.*, **1995**, 709.

14) a) Mukai, K.; Konishi, K.; Nedachi, K.; Takeda, K. *J. Magn. Magn. Mater.*, **1995**, *140-144*, 1449. b) Caneschi, A.; Ferraro, F.; Gatteschi, D. *Adv. Mater.*, **1995**, *7*, 476.

15) Le, L. P.; Keren, A.; Luke, G. M.; Wu, W. D.; Uemura, Y. J.; Tamura, M.; Ishikawa, M.; Kinoshita, M. *Chem. Phys. Lett.*, **1993**, *206*, 405.

16) a) Zheludev, A.; Bonnet, M.; Ressouche, E.; Schweizer, J.; Wan, M.; Wang, H. *J. Magn. Magn. Mater.*, **1994**, *135*, 147-160. b) Zheludev, A.; Ressouche, E.;

Schweizer, J.; Turek, P.; Wan, M.; Wang, H. *Solid State Commun.*, **1994**, *90*, 233-235.

17) McConnell, H. M.; *J. Chem. Phys.*, **1963**, *39*, 1910.

18) a) Hutchison, C. A., Jr.; Kohler, B. E. *J. Chem. Phys.*, **1969**, *51*, 3327. b) Anderson, R. J.; Kohler, B. E. *J. Chem. Phys.*, **1978**, *65*, 2451.

19) a) Izuoka, A.; Murata, S.; Sugawara, T.; Iwamura, H. *J. Am. Chem. Soc.*, **1985**, *107*, 1786. b) Izuoka, A.; Murata, S.; Sugawara, T.; Iwamura, H. *J. Am. Chem. Soc.*, **1987**, *109*, 2631.

20) a) Etter, M. C. *Acc. Chem. Res.*, **1990**, *23*, 120. b) Etter, M. C. *J. Phys. Chem.*, **1991**, *95*, 4601-4610. c) Aakeröy, C. B.; Seddon, K. R. *Chem. Soc. Rev.*, **1993**, 22, 397-407.

21) There are some reports about the magnetic interaction through hydrogen bonds in the transition metal complexes, see: Figgis, B. N.; Kucharski, E. S.; Vrtis, M. *J. Am. Chem. Soc.*, **1993**, *115*, 176-181. and references therein.

22) a) Osiecki, J. H. ; Ullman, E. F. *J. Am. Chem. Soc.*, **1968**, *90*, 1078. b) Ullman, E. F.; Osiecki, J. H.; Boocock, D. G. B.; Darcy, R. *J. Am. Chem. Soc.*, **1972**, *94*, 7049.

23) Neely, J. W.; Hatch, G. F.; Kreilick, R. W. *J. Am. Chem. Soc.*, **1974**, *96*, 652-656.

24) D'Anna, J. A.; Wharton, J. H. *J. Chem. Phys.*, **1970**, *53*, 4047-4052.

25) Zheludev, A.; Barone, V.; Bonnet, M.; Delley, B.; Grand, A.; Ressouche, E.; Rey, P.; Subra, R.; Schweizer, J.; *J. Am. Chem. Soc.*, **1994**, *116*, 2019.

26) Yamaguchi, K.; Okumura, M.; Nakano, M. *Chem. Phys. Lett.*, **1992**,*191*, 237.

27) The crystal structure and the magnetic property of RSNN have been reported briefly by Veciana *et al.* Other some PhNN derivatives having hydroxy group(s)

have been also reported by them. see: a) Hernàndez, E.; Mas, M.; Molins, E.; Rovira, C.; Veciana, J. *Angew. Chem., Int. Ed. Engl.*, **1993**, *32*, 882. b) Cirujeda, J.; Hernàndez, E.; Rovira, C.; Stanger, J. L.; Turek, P.; Veciana, J. *J. Mater. Chem.*, **1995**, *5*, 243-252. c) Cirujeda, J.; Ochando, L. E.; Amigó, J. M.; Rovira, C; Ruis, J.; Veciana, J. *Angew. Chem., Int. Ed. Engl.*, **1995**, *34*, 55. d) Cirujeda, J.; Hernàndez, E.; Panthou, F. L.; Laugier, J.; Mas, M.; Molins, E.; Rovira, C.; Novoa, J. J.; Rey, P.; Veciana, J. *Mol. Cryst. Liq. Cryst.*, **1995**, *271*, 1-12.

28) Recently, the spin densities on the hydroxy groups of HQNN were determined by the high resolution solid state NMR experiment. The result is consistent with result which is described in this paper.: Takeda, S.; Maruda, G.; Oda, A.; Yamaguchi, K.; Matsushita, M. M.; Izuoka, A.; Sugawara, Symposium on Molecular Structure, Fukuoka, Japan, **1996**, Abstr., 2P3a57, p. 312.

29) MOPAC version 6.0: QCPE No. 445, Stewart, J. J. *QCPE Bull.*, **1990**, *10*(4), 86.

30) Lamchen, M.; Mittag, T. W.; *J. Chem. Soc., C* **1966**, 2300.

31) Oda, A.; Kawakami, T.; Takeda, S.; Mori, W.; Matsushita, M. M.; Izuoka, A.; Sugawara, T.; Yamaguchi, K. *Mol. Cryst. Liq. Cryst.*, in press.

32) Computational studies of the intermolecular magnetic interaction in the hydrogen-bridged nitroxides were performed by Yamaguchi *et al.*, see: Kawakami, T; Takeda, S; Mori, W; Yamaguchi, K. *Chem. Phys. Lett.*, **1996**, *261*, 129-137. and references therein.

33) Panthou, F. L.; Luneau, D.; Laugier, J.; Rey, P. *J. Am. Chem. Soc.*, **1993**,*115*, 9095.

34) Thereafter, sevral hydrogen-bonded radical crystals have been reported: a) Okuno, T.; Otsuka, T.; Awaga, K. *J. Chem. Soc., Chem. Commun.*, **1995**, 827. b) Akita, T.; Mazaki, Y.; Kobayashi, K. *J. Chem. Soc., Chem. Commun.*, **1995**, 1861. c) Yoshioka, N.; Irisawa, M.; Mochizuki, Y.; Kato, T.; Inoue, H.; Ohba, S. *Chem.*

*Lett.*, **1997**, 251.

35) Fan, H.; Qian, J.; Yao, J.; Zheng, C.; Hao, Q. *Acta Crystallogr., Sect.* A, **1988**, *44*, 691.

36) Sheldrick, G. M. *Crystallographic Computing 3*; Sheldrick, G. M.; Kruger, C.; Goddard, R., Eds. Oxford University Press: Oxford, U.K., **1985**; p 175.

37) Sakurai, T.; Kobayashi, K. *Rep. Inst. Phys. Chem. Res. (Tokyo)*, **1979**, *55*, 69.

38) Jongh, L. J.; Miedema, A. R. *Adv. Phys.*, **1974**, *23*, 1.

39) Ishikawa, M.; Nakazawa, Y.; Takabatake, T.; Kishi, A.; Kato, R.; Maesono, A. *Solid State Commun.*, **1988**, *66*, 201.

40) The ac magnetic field in the $\chi_{ac}$ measurement in ref. 12 must be corrected to 10 μT.

41) Ishikawa, M.; Muller, J. *Solid State Commun.*, **1978**,*27*, 761.

42) Matsushita, M. M.; Izuoka, A.; Sugawara, T. *Mol. Cryst. Liq. Cryst.*, **1996**, *279*, 139-144.

43) Ichikawa, M. *Acta Crystallogr.*, **1978**, *B34*, 2074-2080.

44) Byrn, S. R.; Curtin, D. Y.; Paul, I. C.; *J. Am. Chem. Soc.*, **1972**, *94*, 890-898.

45) Nakasuji, K.; Sugiura, K.; Kitagawa, T; Toyoda, J.; Okamoto, H.; Okaniwa, K.; Mitani, T.; Yamamoto, H.; Murata, I.; Kawamoto, A.; Tanaka, J. *J. Am. Chem. Soc.*, **1991**, *113*, 1862.

46) Kumai, R; Matsushita, M. M.; Izuoka, A.; Sugawara, T. *J. Am. Chem. Soc.*, **1994**, *116*, 4523.

47) The crystal structures in this thesis are drawn by Moldraw: Molecular graphics for Machintosh, Cense; J.-M. *Tetrahedron Computer Methodology*, **1989**, *2*, 65-71.

# List of Publications

**Parts of this thesis have been published in the following journals:**

[1] Tadashi Sugawara, Michio M. Matsushita, Akira Izuoka, Nobuo Wada, Naoya Takeda, and Masayasu Ishikawa, An Organic Ferromagnet: α-Phase Crystal of 2-(2',5'-Dihydroxyphenyl)-4,4,5,5,-tetramethyl-4,5-dihydro-1*H*-imidazolyl-1-oxy-3-oxide (α-HQNN), *J. Chem. Soc., Chem. Commun.*, **1994**, 1723.

[2] Michio M. Matsushita, Akira Izuoka, and Tadashi Sugawara, Ferromagnetic Spin Ordering Along Intermolecular Hydrogen Bonds of a Hydroquinone Derivative Carrying a Nitronyl Nitroxide, *Mol. Cryst. Liq. Cryst.*, **279**, 139 (1996).

[3] Michio M. Matsushita, Akira Izuoka, Tadashi Sugawara, Tatsuya Kobayashi, Nobuo Wada, Naoya Takeda, and Masayasu Ishikawa, Hydrogen-Bonded Organic Ferromagnet, *J. Am. Chem. Soc.*, in press.

**The following publications are not included in this thesis:**

[1] Masataka Yokoyama, Michio Matushita, Sachiko Hirano, and Hideo Togo, Synthesis of 6-Oxa-1,5-Pentamethylenetetrazoles (Sugar Tetrazoles), *Tetrahedron Lett.*, **34**, 5097 (1993).

[2] Masataka Yokoyama, Sachiko Hirano, Michio Matsushita, Takeshi Hachiya, Naoki Kobayashi, Misao Kubo, Hideo Togo, and Hiroko Seki, Synthesis of tetrazoles bearing a sugar moiety (sugar tetrazoles). X-Ray molecular structure of '(7R,8R,9S,10R)-8,9,10-tribenzyloxy-7-benzyloxymethyl-6-oxa-1,5-pentamethylenetetrazole', *J. Chem. Soc., Perkin Trans. 1*, **1995**, 1747.

[3] Reiji Kumai, Michio M. Matsushita, Akira Izuoka, and Tadashi Sugawara, Intramolecular Exchange Interaction in a Novel Cross-Conjugated Spin System Composed of π-Ion Radical and Nitronyl Nitroxide, *J. Am. Chem. Soc.*, **116**, 4523 (1994).

[4] Akifumi Oda, Takashi Kawakami, Sadamu Takeda, Wasuke Mori, Michio M. Matsushita, Akira Izuoka, Tadashi Sugawara, and Kizashi Yamaguchi, Theoretical Studies on Crystals of 2',5'-Dihydroxyphenyl Nitronyl Nitroxide, *Mol. Cryst. Liq. Cryst.*, in press

[5] Jotaro Nakazaki, Michio M. Matsushita, Akira Izuoka, and Tadashi Sugawara, Ground State Spin Multiplicity of Cation Diradicals Derived from Pyrroles Carrying Nitronyl Nitroxide, *Mol. Cryst. Liq. Cryst.*, in press.

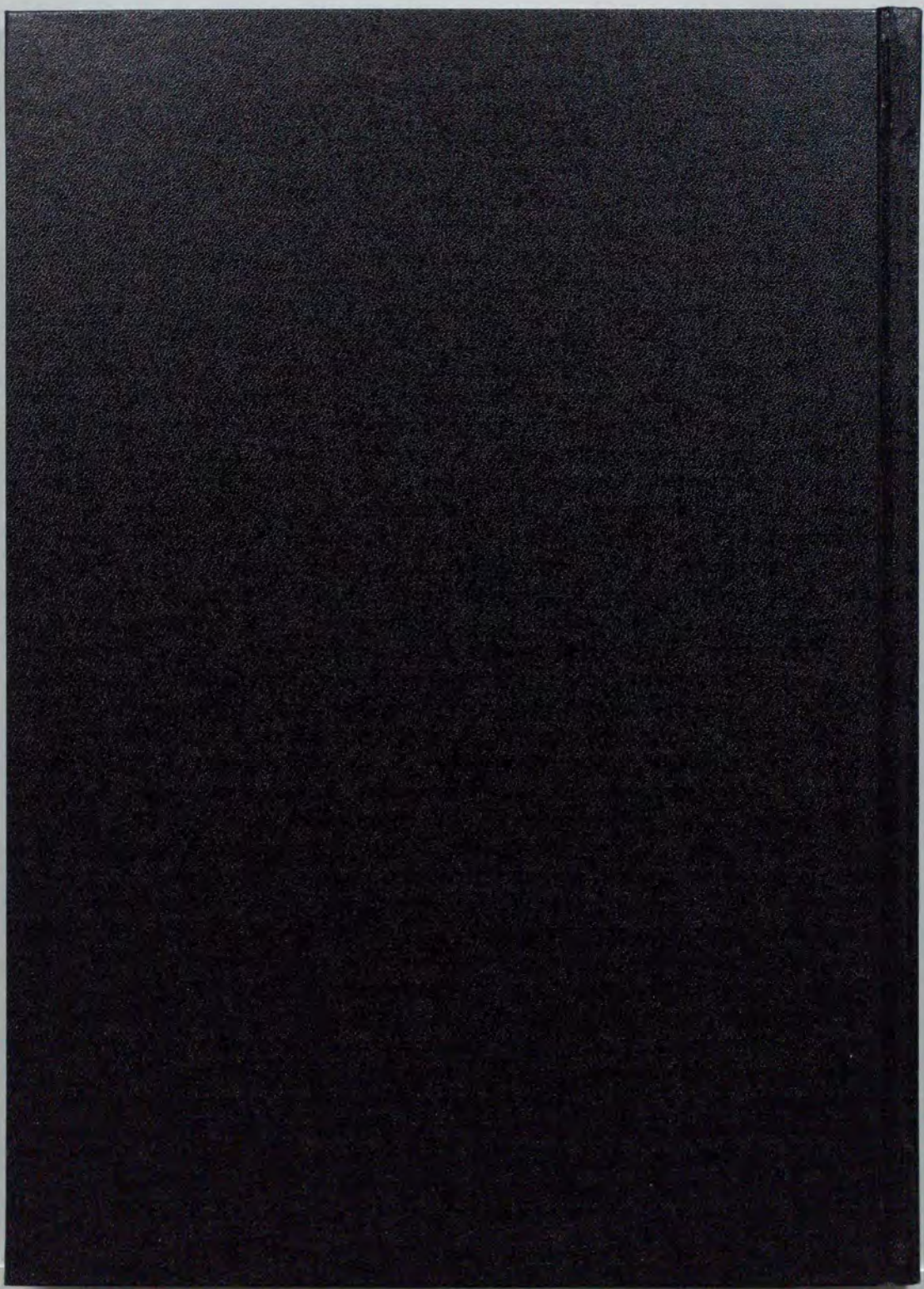

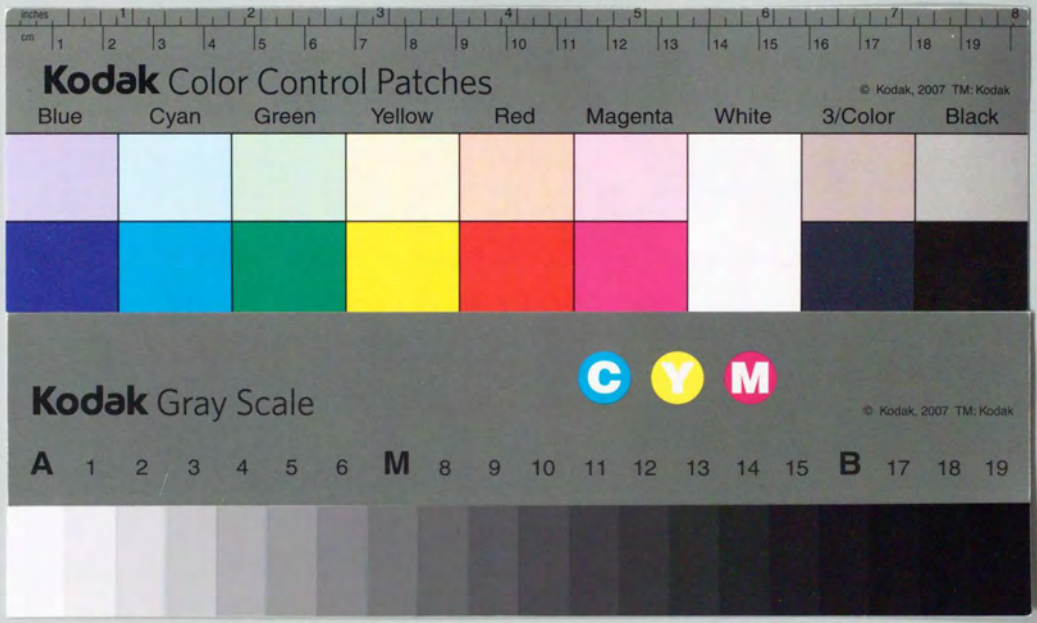
inches
cm
Kodak Color Control Patches
© Kodak, 2007 TM: Kodak
Blue
Cyan
Green
Yellow
Red
Magenta
White
3/Color
Black
Kodak Gray Scale
C
Y
M
© Kodak, 2007 TM: Kodak
A 1 2 3 4 5 6 M 8 9 10 11 12 13 14 15 B 17 18 19